



FCTUC DEPARTAMENTO DE ENGENHARIA CIVIL
FACULDADE DE CIÊNCIAS E TECNOLOGIA
UNIVERSIDADE DE COIMBRA

Structural Behaviour of Post-Tensioned Glass Beams

Dissertação apresentada para a obtenção do grau de Mestre em Engenharia Civil na
Especialidade de Mecânica Estrutural,

Autor

João Pedro Fernandes Olim Neves

Orientadores

Prof. Dr. Sandra Filomena da Silva Jordão Alves

Dr. Eng. Christian Louter

Esta dissertação é da exclusividade responsabilidade do seu autor, não tendo sofrido correções após a defesa em provas públicas. O Departamento de Engenharia Civil da FCTUC declina qualquer responsabilidade pelo uso da informação apresentada.

Coimbra, Setembro, 2014



FCTUC DEPARTAMENTO DE ENGENHARIA CIVIL
FACULDADE DE CIÊNCIAS E TECNOLOGIA
UNIVERSIDADE DE COIMBRA

Structural Behaviour of Post-Tensioned Glass Beams

Dissertation submitted for the degree of Master of Civil Engineering Specialization in
Structural Mechanics,

Author

João Pedro Fernandes Olim Neves

Supervisors

Prof. Dr. Sandra Filomena da Silva Jordão Alves

Dr. Eng. Christian Louter

This dissertation is the sole responsibility of its author, not having suffered corrections after the public thesis presentation. The Department of Civil Engineering FCTUC accepts no responsibility for the use of the presented information.

Coimbra, September, 2014

Acknowledgements

I'd like to acknowledge all professors from the Department of Civil Engineering at the University of Coimbra for teaching me to excel in this field, but in particular a special acknowledgement to Prof. Sandra Jordão for accepting being my tutor and for providing me one of the most important journeys of my whole life. A special acknowledgement to my friend and colleague Marco Pinho for helping in my most desperate moments during the numerical analysis.

Prof. Dr. Jean Paul Lebet is highly acknowledged for hosting me at the great polytechnic school EPFL is. This journey made me a different and more aware engineer. I'd like to acknowledge Dr. Ing. Christian Louter for being my tutor abroad and Jagoda Cupac for helping me when needed and for providing the experimental data.

Last but not least I'd like to acknowledge my parents for their effort into making this journey possible to me, and a special acknowledgement to my girlfriend Natacha for waiting for me while far, with her unconditional love.

Abstract

The demand for transparency in the last decade has been increasing in the construction industry. The need that *man* has to feel the natural light and to have the perfect landscape in buildings has been challenging engineers. So far Glass is the only construction material that can provide such properties.

The brittleness of the material and its low strength are the main disadvantages of glass as a structural component when compared to the standard construction materials. Technological advances were made by scientists and engineers to avoid or postpone these disadvantages, and that is why glass is nowadays widely used throughout the whole world. Lately these technological advances have become so powerful that today is now possible to have buildings in which the structural components, such as beams or columns, are made of glass.

Despite its use, glass is still not fully characterized and researched and that's the main goal of this thesis. Studying the structural behaviour of post-tensioned glass beams is one step forward to fully know the material and thus, to develop the European Standard Code of Glass.

To do this, a Finite Element Analysis was performed and then calibrated with the experimental results from the ongoing Dissertation of the PhD Candidate Jagoda Cupa c from EPFL. Afterwards some key parameters were studied in order to bear the maximum load.

From the results it's shown that this type of beam is a feasible concept and that the numerical analysis is extremely sensitive to some input parameters. Furthermore, it can also be concluded that the reinforcement used on the bottom of the beam has a great influence on the maximum load the beam can bear and the thickness of the adhesive has a great influence on the initial failure.

Resumo

A procura por transparência na última década tem vindo a aumentar na indústria da construção. A necessidade que o *homem* tem de sentir a luz natural e de obter a paisagem perfeita em edifícios tem vindo a desafiar os engenheiros. Até hoje o vidro é o único material que pode ministrar tais propriedades.

A fragilidade do material e a sua baixa resistência são as principais desvantagens do vidro como componente estrutural quando comparados com os materiais comumente utilizados. Avanços tecnológicos foram feitos por cientistas e engenheiros de modo a evitar ou retardar estas desvantagens, e é graças a esses avanços que o vidro é nos dias de hoje amplamente utilizado pelo globo. Ultimamente esses avanços têm sido tão poderosos que já é possível a existência de edifícios em que até os componentes estruturais, tais como os pilares e as vigas, são feitas de vidro.

Embora já seja utilizado, o vidro não está ainda totalmente caracterizado e investigado e é esse o principal objetivo desta tese. Estudar o comportamento estrutural de vigas de vidro pós-tensionadas é um novo passo nesta caminhada para conhecer por completo o material e assim desenvolver o Eurocódigo de Vidro.

Para efetuar este estudo, uma análise de elementos finitos foi realizada e então calibrada com resultados experimentais da Dissertação da candidata a doutora Jagoda Cupac da EPFL. Depois alguns parâmetros chave foram estudados para que estas vigas possam suportar o máximo de carga.

A partir dos resultados chegou-se à conclusão que este tipo de viga é um conceito viável e que a análise numérica é extremamente sensível a alguns parâmetros de input. Além disso, pode-se concluir que o reforço utilizado no fundo da viga tem uma grande influência na carga máxima que a viga pode suportar e que a espessura do adesivo tem uma grande influência na falha inicial.

Table of Contents

Acknowledgements	i
Abstract	ii
Resumo	iii
Table of Contents	iv
List of Figures	vi
List of Tables	viii
Symbols	ix
1 Introduction	1
1.1 Main Goal of this Thesis	2
1.2 Structure of the Thesis.....	2
2 Overview	3
2.1 Historical evolution of glass.....	3
2.2 Recent technological highlights leading to structural glass.....	4
2.2.1 Float Glass.....	4
2.2.2 Laminated Glass	5
2.2.3 Heat Strengthened Glass.....	6
2.3 The strength of glass	7
2.4 Material properties of glass.....	8
2.4.1 Chemical properties.....	9
2.4.2 Optical Properties	9
2.4.3 Physical properties	10
3 State of art on glass beam systems	12
3.1 Structural behaviour.....	12
3.1.1 Reinforced Glass Beams.....	12
3.1.2 Post-tensioned Glass Beams	12
3.1.3 Tempered Glass Beams vs Laminated Glass Beams	13
3.2 Overview of similar post-tensioned beams.....	14
4 Experimental Analysis	19
4.1 Introduction.....	19
4.2 Layout and instrumentation.....	20
4.3 Materials	21
4.3.1 Glass	21
4.3.2 Stainless Steel.....	21
4.3.3 Adhesive.....	22
4.3.4 Interlayer material	23
4.4 Loading	24
4.5 Structural Model.....	24
4.6 Results	25
5 Numerical Analysis	27
5.1 Structural model	27

5.2	Element type	27
5.3	Explicit Analysis	28
5.4	Quasi-Static Simulation	30
5.5	Reducing the computational cost	31
5.5.1	Speeding up the simulation	31
5.5.2	Using Mass Scaling	31
5.6	Influence of the interlayer in the numerical analysis	34
5.7	Mesh	34
5.8	Equivalent Cross Section	36
5.9	Pre-Stress	37
5.10	Loading Step	40
5.11	Materials' Properties	40
5.11.1	Adhesive Properties	40
5.11.2	Steel Properties	41
5.11.3	Glass Properties	42
5.11.3.1	Mode I fracture Energy	42
5.11.3.2	Brittle Shear	45
5.11.3.3	Brittle Failure	50
6	Parametric Study	51
6.1	Thickness of the Adhesive	51
6.2	Characterization of the Steel	52
7	Conclusions	54
7.1	Suggestions for future research	54
8	Bibliographic References	55

List of Figures

FIGURE 2.1 – FLOAT PROCESS (HALDIMANN ET AL., 2008)	4
FIGURE 2.2 – LAMINATED GLASS PROCESS	5
FIGURE 2.3 – STRUCTURAL PERFORMANCE VS REMAINING STRUCTURAL CAPACITY IN LAMINATED GLASS (HALDIMANN ET AL., 2008).....	5
FIGURE 2.4 – INTERNAL FORCES IN ANNEALED [LEFT] AND TEMPERED [RIGHT] GLASS (HALDIMANN ET AL., 2008)	6
FIGURE 2.5 – FRACTURE PATTERNS OF ANNEALED [LEFT], TEMPERED [MIDDLE] AND FULLY TEMPERED [RIGHT] GLASS (HALDIMANN ET AL., 2008).....	7
FIGURE 2.6 – COMPRESSIVE STRESSES ARE USUALLY ACCOMPANIED BY TENSILE STRESSES.....	8
FIGURE 2.7 – A) CHEMICAL COMPOSITION OF SLSG AND BSG; B) NETWORK OF SLSG (HALDIMANN ET AL., 2008)	9
FIGURE 2.8 – TRANSMITTANCE AS A FUNCTION OF WAVELENGTH (HALDIMANN ET AL., 2008)	10
FIGURE 3.1 – REINFORCED GLASS BEAM CROSS SECTION AND ITS DUCTILITY (LOUTER, 2011)	12
FIGURE 3.2 – TRACTION CAPACITY VS COMPRESSION CAPACITY (ADAPTED FROM DIAZ ET AL., 2011).....	13
FIGURE 3.3 – INTERNAL FORCES OF THE CROSS SECTION BEFORE LOADING	13
FIGURE 3.4 – REMAINING LOAD CARRYING CAPACITY AFTER FIRST CRACK BETWEEN ANNEALED AND TEMPERED GLASS (LOUTER, 2011)	14
FIGURE 3.5 – T-SECTION BEAM LAYOUT [LEFT] AND CROSS SECTION [RIGHT] (LOUTER, 2008).....	14
FIGURE 3.6 – HYBRID PRE-STRESSED STEEL-GLASS BEAM (FROLI & LANI, 2010)	15
FIGURE 3.7 – LAMINATED GLASS BEAM REINFORCED WITH PRE-STRESSED CABLES (JORDÃO ET AL., 2014)	15
FIGURE 3.8 – 4 TYPES STUDIED IN (WELLER & ENGELMANN, 2014)	16
FIGURE 3.9 – LAYOUT OF THE TYPE B AND TYPE D BEAMS (WELLER & ENGELMANN, 2014)	16
FIGURE 3.10 – OUT OF PLANE DISPLACEMENT (WELLER & ENGELMANN, 2014)	16
FIGURE 3.11 – POST-TENSIONED BEAMS TESTED IN (LOUTER, 2013).....	17
FIGURE 3.12 – STRUCTURAL BEHAVIOUR OF TWO GLASS BEAMS. (LOUTER, 2013).....	17
FIGURE 3.13 – FORCE VS DISPLACEMENT PLOT (FROLI & MAMONE, 2014)	18
FIGURE 4.1 – STRUCTURAL MODEL OF THE BEAM.....	20
FIGURE 4.2 – CROSS-SECTION DETAILS	20
FIGURE 4.3 – NOMINAL CURVE FOR AISI 304.....	22
FIGURE 4.4 – STRUCTURAL BEHAVIOR OF THE ADHESIVE ACCORDING TO (NHAMOINESU AND OVEREND, 2012)	22
FIGURE 4.5 - PROPERTIES OF SGP DEPENDING ON TIME OF LOAD AND TEMPERATURE (STELZER, 2010).....	23
FIGURE 4.6 - UNLOADED BEAM (LEFT), LOADED BEAM (RIGHT).....	24
FIGURE 4.7 - STRESS DISTRIBUTION AFTER THE CRACKING	24
FIGURE 4.8 – INTERNAL FORCES DUE TO THE PRE-STRESS STEP.....	25
FIGURE 4.9 – INTERNAL FORCES DUE TO THE LOADING STEP.....	25

FIGURE 4.10 - PROVIDED DATA FROM EXPERIMENTS IN REINFORCED GLASS BEAMS (LEFT) AND POST-TENSIONED GLASS BEAMS (RIGHT).....	26
FIGURE 4.11 – DIFFERENCE BETWEEN THE REINFORCED BEAM BEHAVIOR AND THE POST-TENSIONED BEAM BEHAVIOR	26
FIGURE 5.1 - REPRESENTATION OF THE BOUNDARY CONDITIONS	27
FIGURE 5.2 - PURPOSES OF BOTH ANALYSIS (MASHAYEKHI, 2013)	29
FIGURE 5.3 - AMPLITUDE IMPOSED	30
FIGURE 5.4- REACTION FORCE IN FUNCTION OF TIME WHEN STEP TIME WAS 1 COMPUTATIONAL SECOND.....	32
FIGURE 5.5 - REACTION FORCE IN FUNCTION OF TIME WHEN STEP TIME WAS 50 COMPUTATIONAL SECONDS	33
FIGURE 5.6 – THE INFLUENCE OF THE SGP IN FORCE-DISPLACEMENT CURVES (LOUTER ET NIELSEN, 2013).....	34
FIGURE 5.7 – MESH PATTERN USED IN BEDON AND LOUTER, 2014	35
FIGURE 5.8 – MESH PATTERN USED WITHIN THIS STUDY	35
FIGURE 5.9 – ZOOMED PICTURE OF THE MESH USED WITHIN THE STUDY AT THE BOTTOM EDGE OF THE BEAM	35
FIGURE 5.10 – DIFFERENCES BETWEEN THE REAL [O] AND THE NUMERICAL CROSS SECTIONS [A, B AND C]	36
FIGURE 5.11 – FORCE-DISPLACEMENT CURVES FROM EXPERIMENT [O] AND NUMERICAL ANALYSIS [A, B AND C]	37
FIGURE 5.12 – FORCE ANALOGY REGARDING THE PRE-STRESS	38
FIGURE 5.13 – STRESS ON THE STEEL ALONG ITS AXIS AND ITS AXIAL FORCE DUE TO THE FORCE ANALOGY	38
FIGURE 5.14 – STRESS ON THE STEEL ALONG ITS AXIS AND ITS AXIAL FORCE DUE TO THE VARIATION OF TEMPERATURE	39
FIGURE 5.15 – CONNECTION BETWEEN THE BEND RADIUS AND THE HALF SPAN DISPLACEMENT.....	40
FIGURE 5.16 - ADHESIVE BEHAVIOUR STUDY	41
FIGURE 5.17 – COMPARISON BETWEEN THE EXPERIMENTAL RESULTS AND THE FEM RESULTS WITH THE STEEL CHARACTERIZATION ACCORDING TO LOUTER, 2011.....	42
FIGURE 5.18 - MODE I FRACTURE ENERGY (AREA)	43
FIGURE 5.19 - DIFFERENT FRACTURE MODES (TWISP, 2008).....	43
FIGURE 5.20 – MODE I FRACTURE ENERGY IN GLASS.....	44
FIGURE 5.21 – EFFECTS OF FRACTURE ENERGY OF GLASS. COMPARISON OF LOAD-DISPLACEMENT PLOTS [LEFT]; COMPARISON OF CRACK PATTERNS [RIGHT] (BEDON AND LOUTER, 2014).....	45
FIGURE 5.22 - SHEAR RETENTION FACTOR (ρ) VARIES WITH CRACK STRAIN OPENING (E^{CK})	46
FIGURE 5.23 – SHEAR RETENTION FACTOR PARAMETER STUDY	47
FIGURE 5.24 - SHEAR RETENTION FACTOR STUDY	48
FIGURE 5.25 - INFLUENCE OF THE E_{MAXCK}	48
FIGURE 5.26 - COMPARISON BETWEEN $E_{MAXCK}=0.1$, $E_{MAXCK}=0.01$ AND $E_{MAXCK}=0.05$	49
FIGURE 5.27 - DIFFERENCE BETWEEN $E_{MAXCK}=0.05$ AND $E_{MAXCK}=0.04$	49
FIGURE 6.1 – RESULTS OF THE PARAMETER STUDY REGARDING THE THICKNESS OF THE ADHESIVE	52
FIGURE 6.2 - RESULTS OF THE PARAMETER STUDY REGARDING THE CHARACTERIZATION OF THE STEEL.....	53

List of Tables

TABLE 2.1 – PROPERTIES OF DIFFERENT MATERIALS (ADAPTED FROM WURM, 2007)	11
TABLE 2.2 – MECHANICAL PROPERTIES OF SLSG AND BSG (ADAPTED FROM HALDIMANN ET AL., 2008)	11
TABLE 4.1 – EXPERIMENTAL STUDY.....	19
TABLE 4.2 – NOMINAL VALUES FOR AISI 304 (ADAPTED FROM LOUTER, 2011)	22
TABLE 5.1 – ANALYSIS TYPE AND MESH STUDY.....	28
TABLE 5.2 - ANALYTICAL VS NUMERICAL APPROACH REGARDING THE PRE-STRESS	40
TABLE 5.3 – FRACTURE ENERGY STUDY DONE IN (BEDON AND LOUTER, 2014).....	44
TABLE 5.4 – SHEAR RETENTION FACTOR PARAMETER VARIATION	47
TABLE 6.1 – THICKNESSES OF THE ADHESIVE STUDIED	51
TABLE 6.2 – INITIAL FAILURE AND MAXIMUM LOAD OF THE THICKNESS OF THE ADHESIVE STUDY	52
TABLE 6.3 – STEEL STUDY	53
TABLE 6.4 - INITIAL FAILURE AND MAXIMUM LOAD OF THE STEEL CHARACTERIZATION STUDY	53

Symbols

Latin letters:

a	acceleration
A	Cross-sectional area of the whole beam
A_i	Cross-sectional area of the considered element
A_s	Cross-Sectional Area of the steel
I_{yy}	Moment of Inertia in its strong axis
e_{max}^{ck}	Maximum crack strain
e_{nn}^{ck}	Crack strain
E_g	Young's Modulus of Glass
E_i	Young's Modulus of the considered component in the section
E_s	Young's Modulus of Steel
$EI_{composite}$	Bending Stiffness of the composite section
C_d	Dilatational wave speed
f_t	Ultimate Tensile Strength
$f_{y0,2\%}$	Yield Strength 0.2% Proof
F	Force
$g.c.$	Geometrical Centre
G	Shear Modulus
G_f	Mode I fracture Energy
i	considered component in the section
I_{yy}	Moment of Inertia in its strong axis
$I_{yy,i}$	Moment of Inertia of the considered component in its strong axis
L	Length of the beam
L_{min}	smallest element dimension in the mesh
m	mass
M_{Load}	Moment due the loading in the moment of the 1 st crack
M_{PS}	Equivalent Moment due the pre-stress
n	Total number of components in the section
N	Pre-Stress
r_0	Equilibrium spacing of the atom
u_{ck}	Critical Displacement
v	Distance from the geometrical centre of the beam to the top of the glass
z_i	distance between the axis of the considered component and the neutral axis

Greek Letters:

α	Coefficient of thermal expansion
γ	Fracture Surface Energy
ΔT	Variation of Temperature
ε	Extension
λ_0	Lamé's first parameter
ν	Poisson's Ration
ρ	Shear Retention Factor
ρ_r	Bending radius
σ	Stress
$\sigma_{c, glass}$	Failure Stress of Glass
σ_m	Theoretical failure stress
μ_0	Lamé's second parameter (also called Shear Modulus)

1 Introduction

Glass by itself is an extraordinary product because it allows the entrance of light and an unobstructed view of any landscape. Many buildings still lack the possibility to have natural light instead of artificial light due to the lack of glass in its façades.

Glass demanding has been increasing. The use of glass in buildings it's getting more and more often and the dimensions of these components have been increasing due to the successive technological advances. Such technological advances has made glass as affordable as it never was.

There has been so many technological advances in the last decade that glass is now becoming a structural material, i.e., instead of the standard materials such as steel or concrete, there are now buildings in which the columns and/or the beams are made of glass.

In order to get the needed confidence of the projects designers and the developers this material and its behaviour needs to be well known and characterized. That's the role of this research. The present thesis aims to contribute to the whole knowledge of the product and the structural behaviour of post tensioned glass beams.

The structural model of post tensioned glass beams when compared with normal glass beams is advantageous as it has a higher load bear capacity and it slows the propagation of the cracks in the material due to the steel in the tensile zone.

The work in the present theses has been done with the following methodology:

1. Experiments
2. Finite Element Analysis
3. Calibration
4. Parametrical Study

It should be noticed that the research for this thesis was performed at EPFL (Switzerland). There experimental data was provided so it can be used to calibrate with the numerical modelling. This data was obtained to be also used in the Dissertation of the PhD Candidate Jagoda Cupać from EPFL.

1.1 Main Goal of this Thesis

The purpose of the present thesis is to contribute to the characterization of the behaviour of post-tensioned glass beams. The approach chosen for such aim encompasses the preparation of a numerical element model of the beam, duly calibrated with the experimental results given by (Cupać, 2014). The calibrated numerical model was then used to perform a parametrical analysis on the main/key parameters conditioning the structural behaviour of the beam system.

The main outcome is a toll (FEM of the beam) that is ready to validate any new design formulations for this structural system, or to allow broader parametric analysis, bringing in a clearer view on the structural behaviour. This is in fact a valid input/iteration for the characterization of post-tensioned glass beams.

1.2 Structure of the Thesis

In the second chapter there's an overview of the study done in glass and the technologies involved. This study regards a historical evolution of glass and some ways to enhance the strength or the safety of glass, the mechanical and chemical properties of glass and its strength.

Chapter 3 concerns the state of the art on glass beam systems such as their structural behaviour, and a brief overview of some similar post-tensioned glass beams, in which the cross-section and the main conclusions of the research are included.

In Chapter 4 information regarding the experimental analysis can be found. There is also the properties of the materials used in the beam, the structural model and its internal forces and a summary of the results.

In Chapter 5 the structural model of the numerical analysis may be found, as well as the elements type used for each material, the cross section used, an explanation why a certain type of analysis was used, the parameters input in the software and how their values were obtained, the mesh used in the FEA, the method used to simulate accurately the experiments done, how the computational cost was reduced and its consequences and the method used the simulate the pretension of the beam.

In Chapter 6 a parametrical study may be found as well as some commentaries regarding this study and the results obtained, and in Chapter 7 there's an overall conclusion about the numerical analysis and the parametrical study. Some suggestions for future study is also present in this chapter.

2 Overview

2.1 Historical evolution of glass

Glass began being manufactured nearly 3500 years ago, yet slowly due to the limited techniques available. It was the Egyptians and Mesopotamians the pioneers of glass manufacturing with glass beads and vessels. About the next millennium glass manufacturing became widely practiced, with improvements in its manufacturing such as new ingredients to improve its strength or produce clearer glass. Such techniques was yet difficult and expensive so almost only royalty or religious services used glass. Near 300 B.C. the first revolution of glass appeared due the discovery of the Syrians' new blow pipe. Due to the ease of the process the price of glass dropped and such discovery made the glass affordable to the average citizen. (Kennedy, 1997)

In the first century A.D. the romans revolutionized glass making by a using a variety of manufacturing processes. Their geography couldn't be better; their market were everywhere because of the great Roman Empire. They were the first to apply a silver amalgam to flat glass to manufacture mirrors. Thanks to these Romans, glass industry spread throughout Europe but, as the Roman Empire falls, so do the fine art of glass making and the glass became again a product for the wealthy, and flat glass was now used to medieval churches. In 650 A.D. Syrian glassmakers developed a new manufacturing method for producing "crown glass". This glass was used in windows and they were made by the blown glass through a "crown". Then it was flattened by reheating and as it was spinning it creates a "bulls eye" thanks to centrifugal force. (Carter and Norton, 2007) This type of glass was used in windows until the late 19th century. (Kennedy, 1997)

In the late 13th century Venetians entered the glass industry. Until then they had been importing Byzantine glassware. The Industry by that time was already challenging and they had to move all Venetian glasshouses to the Island of Murano in order to protect "trade secrets". They also created a way to perfect the plate glass by casting colourless glass on an iron table and polishing the glass until no distortions remained. It was so profitable to these venetians that the city fathers instituted death penalty for anyone who revealed the secret behind the manufacturing process. Eventually the Venetian glassmaking expertise spread throughout Europe and France improved upon Italian processes only by using larger tables and creating annealing ovens that gave French glassmakers a way to cool glass sheets over the course of several days. (Kennedy, 1997)

Glass makers, in the 1900s, discovered a way to improve glass strength by as much as 400% by tempering it. Such improve was important for automotive industries. Due to the housing and automobile boom after the World War I the flat glass industry grown exponentially. The mainly used glass was still flat, despite its high price. So the glassmakers tried to achieve a new kind of cheaper glass. Alastair Pilkington succeeded in this manner by developing the modern float glass process between 1953 and 1957 that eliminates the distinction between flat and polished plate glass. Companies that were capable to produce glass with this new improved process were increasing their capacity, lowering the price of glass, though smaller firms that could not use such innovative process had leading difficulties. (Kennedy, 1997)

2.2 Recent technological highlights leading to structural glass

This chapter concerns technological aspects and improvements of glass. It's important to mention that is due to such improvements that one is now able to create an entire building made of glass.

2.2.1 Float Glass

The main production process for flat glass in the current days is the float process. Such continuous process consists on the melting of raw materials in a furnace at 1550 °C, then the molten glass is poured at 1000 °C onto a bath of molten tin. In this tin the glass floats due to the difference between the glass' density and the molten tin's density, forming a glass ribbon with smooth surfaces. The wanted thickness of the glass can be easily adjusted by the top rollers; the faster they roll, the thinner the glass will be and vice-versa. When the glass has passed through the whole tin bath it should be around 600 °C, and is drawn into an annealing lehr, in which the main objective is to cool down the glass slowly (from 500 °C to 100 °C), in order to prevent residual stresses. After this whole process the glass should be perfectly functional, so there's an automated inspection right after the end of the annealing lehr and then the final cutting of the glass. In Figure 2.1 it's shown a schematic representation of the float glass process. (Haldimann et al., 2008)

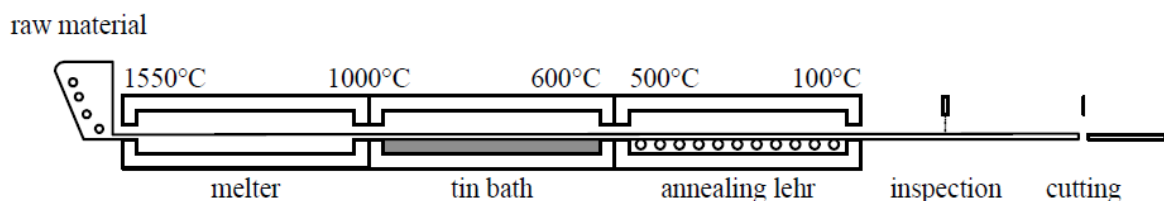


Figure 2.1 – Float Process (Haldimann et al., 2008)

2.2.2 Laminated Glass

One of the ways engineers found to enhance the security of glass is by laminating it, i.e., bonding two or more layers of glass. (Figure 2.2) By bonding the full-surface many opportunities are provided to modify the mechanical properties of the section. Laminated glass remains as one piece when shattered – after breakage, the glass fragments adhere to the film and so a certain remaining structural capacity is obtained. (Wurm, 2007) This post-breakage behaviour furthermore depends on the interlayer material and its properties. (Haldimann et al., 2008)

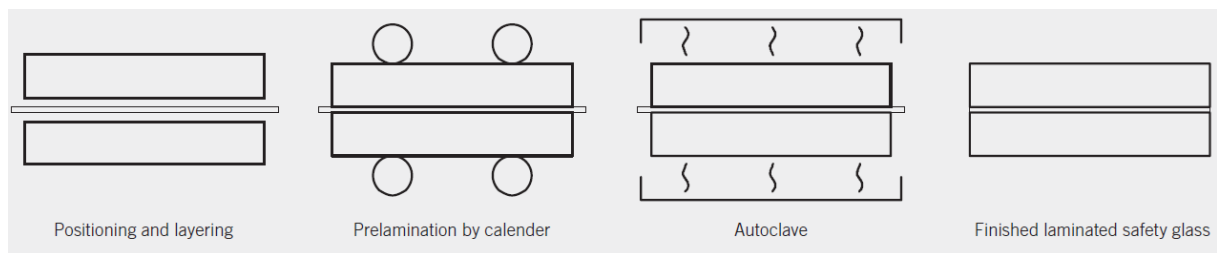


Figure 2.2 – Laminated Glass Process

The remaining load capacity is dependent on the fragmentation of glass, i.e., the bigger the fragments the better the post-breakage behaviour. Such property asks for extreme care when dealing with the different types of glass. Although it's well known that tempered glass has a higher strength than annealed glass, it has also a higher energy stored (see 2.2.3) that makes it shatter in pieces when the strength is surpassed. Annealed glass, since has no energy stored, breaks in larger fragments. Thus, the remaining structural capacity in annealed laminated glass is better than that of tempered laminated glass. (Haldimann et al., 2008)

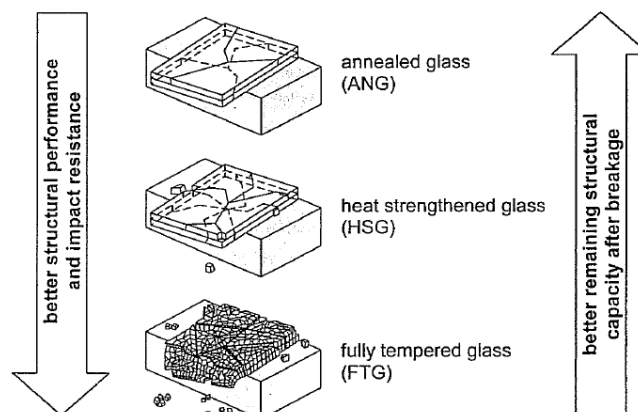


Figure 2.3 – Structural performance vs remaining structural capacity in laminated glass (Haldimann et al., 2008)

Although the interlayer is not a rigid material, it is fundamental so the whole section can work as one. Despite its viscoelastic behaviour it has proven to be an asset regarding the structural behaviour of laminated glass.

One suggestion from the bibliography is that, for the usual interlayers, we can assume a full composite shear section stiffness exclusively for short-term loads such as wind or impact. This means that for permanent loads such as dead load it should only be considered the stiffness of the individual sheets. (Wurm et al., 2007)

The first interlayers to have a widespread use as laminating adhesive was Polyvinyl butyral film, also known as PVB. Its main drawback is that it is strongly dependent from the duration of the load and the temperature. At 80°C the PVB film starts to delaminate. A new product has become available that overcomes negative features of PVB. Sentry Glass Plus, also known as SGP, which has a stiffness up to 100 times higher than that of the common PVB, it is less temperature dependent and can carry the same load with thinner thicknesses. With this type of interlayer the full interaction can be assumed even for permanent loads. (Wurm, 2007)

2.2.3 Heat Strengthened Glass

One of the ways to enhance the strength of the glass is by tempering it. This process consists in rapidly cooling the glass causing the surface to cool faster than the interior, which produce compression stresses at the surface and tension stresses at the interior of the glass. This compression is beneficial because it is like a pre-stress field which tends to avoid the spreading of the crack. (Figure 2.4) This pre-stress compression field brings in a higher energy stored at the glass which once damaged, shatters in tiny pieces. (Haldimann et al., 2008)

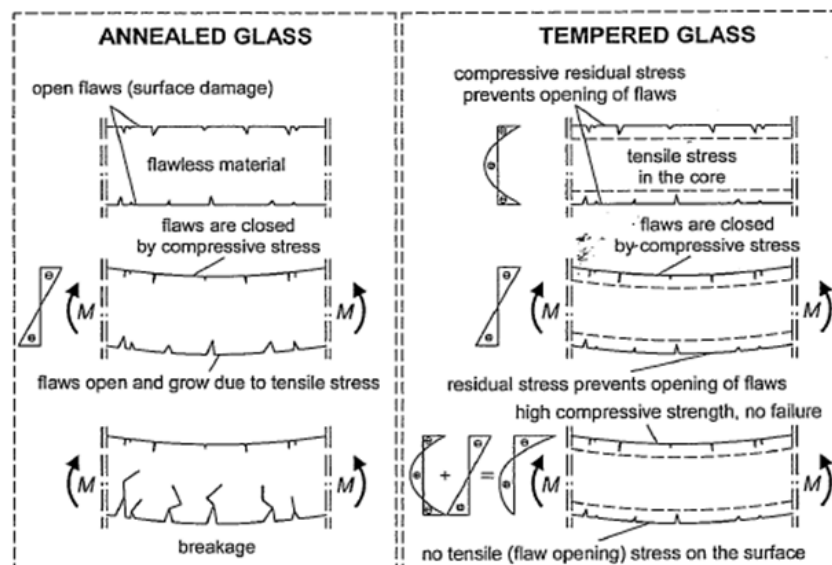


Figure 2.4 – Internal forces in Annealed [left] and Tempered [right] Glass (Haldimann et al., 2008)

The difference between annealed, tempered glass and fully tempered glass is shown by the fracture pattern that they produce. (Figure 2.5) This pattern depends on the energy stored in the glass. Due to the pre-stress observed in the tempered glass, it has the highest fragmentation than that of annealed glass as it is clearly visible in the following figures. It should be noticed that the difference between the figure at the middle, and the picture at the right is the temperature gradient during the tempering process. (Haldimann et al., 2008)

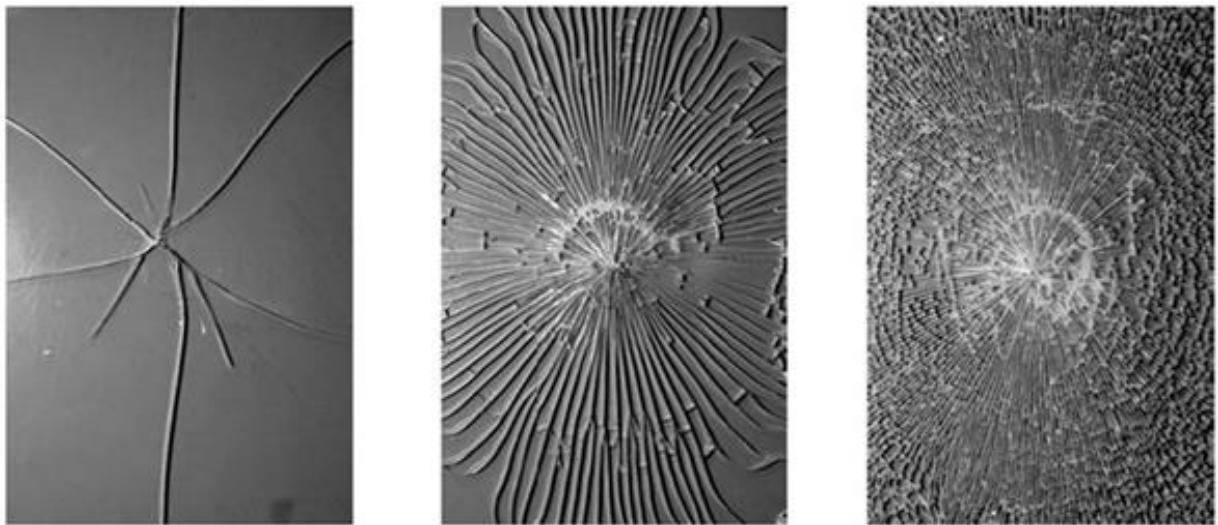


Figure 2.5 – Fracture patterns of Annealed [Left], Tempered [Middle] and Fully Tempered [Right] Glass (Haldimann et al., 2008)

2.3 The strength of glass

The glass strength, as given by the Orowan equation, which is determined by the forces of the interatomic bonds, the theoretical failure stress, σ_m , also known as the stress necessary to break a bond, is about 32 GPa .

$$\sigma_m = \sqrt{\frac{E_g \gamma}{r_0}} \quad (2.1)$$

Where $E_g = 70 \text{ GPa}$, $\gamma = 3 \text{ J/m}^2$, and $r_0 = 0.2 \text{ nm}$ stand for Young's modulus, Fracture Surface Energy and Equilibrium spacing of the atoms, respectively.

Obviously, the real tensile strength is much lower, and this huge difference between the theoretical and the practical strength is, according to Griffith, due the microscopic flaws at the glass surface that are unnoticeable to the naked eye. These microscopic flaws are already present right after the production process of glass. Additional flaws may occur in the further processes until installation and even in its service life-time. The strength is highly related to the flaw dimension (depth). Despite the bending strength of annealed glass varies between 30 and 80 MPa (Feldmann and Kasper, 2014), in the bibliography the most common value for the strength of glass in tension is 45 MPa. (Louter, 2011) This value is given with a 5% breakage probability and a confidence interval of 95%. (Valarinho, 2010)

Crack opening and propagation are prevented in compression, thus the glass compressive strength is up to 900 MPa, but compressive stresses are usually accompanied by tensile stresses. An element when compressed has an equivalent moment due to the offset between the point where the compression is applied and the gravity centre of the cross-section. (Figure 2.6) Due to this effect the actual compressive strength, as given in the literature, is about 500 MPa. This compressive strength, decreases to 170 MPa when under permanent loads given the creep behaviour of viscoelastic materials under such loads. (Wurm, 2007)

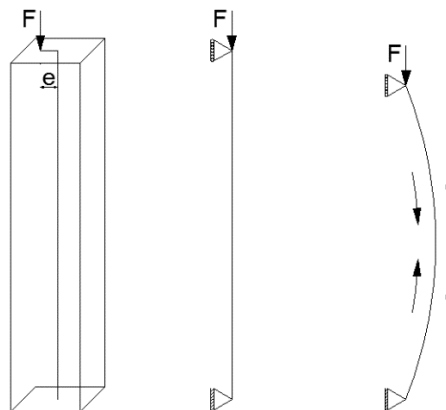


Figure 2.6 – Compressive stresses are usually accompanied by tensile stresses

2.4 Material properties of glass

Glass is a solid, inorganic, homogeneous product of fusion. (Valarinho, 2010) Given the quick cooling it forms without crystallization, and that's the reason it is often called *supercooled liquid*. Materials with non-crystalline molecular structure are called amorphous. (Wurm, 2007)

2.4.1 Chemical properties

There are two major types of glass: soda lime silica glass (SLSG) and borosilicate glass (BSG). The BSG it's preferred in labs given the heat resistance it provides (Haldimann et al., 2008). Both use Silica sand in high quantities (Figure 2.7a) which is present in the Earth's crust in the form of pure quartz sand. (Wurm, 2007) Glass, unlike most other materials, do not consist of a geometrically regular network of crystals. (Haldimann et al., 2008)

		Soda lime silica glass	Borosilicate Glass
Silica sand	SiO ₂	69-74%	70-87%
Lime (calcium oxide)	CaO	5-14%	-
Soda	Na ₂ O	10-16%	0-8%
Boron-oxide	B ₂ O ₃	-	7-15%
Potassium oxide	K ₂ O	-	0-8%
Magnesia	MgO	0-6%	-
Alumina	Al ₂ O ₃	0-3%	0-8%
Others		0-5%	0-8%

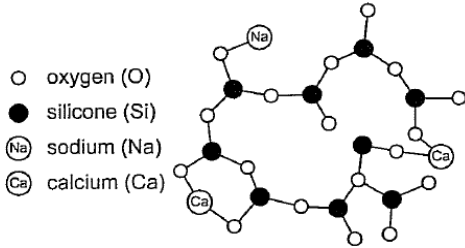


Figure 2.7 – a) Chemical composition of SLSG and BSG; b) Network of SLSG (Haldimann et al., 2008)

2.4.2 Optical Properties

Unlike most solids, the electrons in glass are confined to particular energy levels, i.e., the molecules cannot alternate between different states of excitement by absorbing radiation in the bandwidths of visible and near infrared. Thus, the molecules do not absorb or dissipate those forms of radiant energy and so, the energy passes without interaction with the molecules of the material and hence glass appears transparent. As impurities aren't unavoidable in the soda-lime silica mix, typical windows absorb some radiation due to small amounts of iron that oxides causing a greenish colour of SLSG. This unwanted effect can be avoided using extra-clear glass, also known as low iron glass. (Haldimann et al., 2008)

Despite its disadvantages when compared with other materials, glass is able to give a high transparency within the visible range of wavelengths ($\lambda = 380-750\text{nm}$) that no other material can. Within the Ultraviolet range and the infrared range the glass absorbs radiation due to interaction with O₂-ions in the glass and Si-O-groups, respectively. (Figure 2.8) (Haldimann et al., 2008)

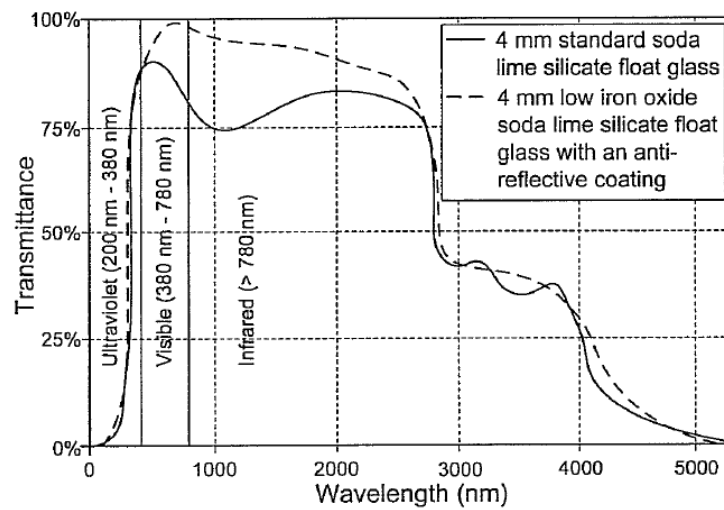


Figure 2.8 – Transmittance as a function of wavelength (Haldimann et al., 2008)

2.4.3 Physical properties

The main disadvantage of glass, is that it is brittle, and cracks can easily propagate through it. That's because when this material is bent there's compression stress on one side of the surface, and tension stress on the other side of the surface. That tension stress opens the crack and pulls it through the slide, resulting in fracture. Metals on the other hand are generally ductile, meaning that when it's bent the atoms can distribute the higher stresses, and consequently cracks have a hard time travelling through metals. In order to make the glass used in construction and other industries, engineers had to think of ways of making glass more fracture resistant. (Haldimann et al., 2008)

In Table 2.1 there are the mechanical properties of different construction materials and the reasons why glass should be handled with care; and in Table 2.2 the mechanical properties of SLSG and BSG.

Table 2.1 – Properties of Different Materials (adapted from Wurm, 2007)

	Steel S 235	Softwood S 10	Concrete C20/25	Glass Soda-lime glass
Refractive index η	-	-	-	1.5
Density ρ [kN/m ³]	78.5	6	22	25
Modulus of Elasticity E [kN/cm ²]	21000	1100	2900	7000 (like aluminium)
Tensile strength $f_{t,k}$ [kN/cm ²]	24 (yield strength)	1.4	0.22	4.5
Elongation at break ε in %	25	0.7	-	0.006 - 0.17
Compressive strength $f_{c,k}$ [kN/cm ²]	23.5	1.8-2.6 ⊥ 0.4-0.6	2	approx.50
Limiting tensile stress $\sigma_{II,d}$	21.8	0.9	(-0.1)	1.2/1.8
Safety factor γ	1.1	1.3	1.8	2.5
Breaking length s/r [m]	2800	1500	-45	480/720
Thermal conductivity [W/m x K]	75	0.5 ⊥ 0.5	1.6	1
Thermal shock resistance ΔT [1/K]	-	-	-	40
Coefficient of thermal expansion α_t [1/K]	12×10^{-6}	5×10^{-6} ⊥ 35×10^{-6}	10×10^{-6}	9×10^{-6} 60 K \approx 0.5mm/m

Table 2.2 – Mechanical properties of SLSG and BSG (adapted from Haldimann et al., 2008)

			Sola lime silica glass	Borosilicate Glass
Density	ρ	kg/m ³	2500	2200-2500
Knoop hardness	HK _{0,1/20}	GPa	6	4.5-6
Young's modulus	E	MPa	70000	60000-70000
Poisson's ratio	ν	-	0.23	0.2
Coefficient of thermal expansion	α_t	$10^{-6}K^{-1}$	9	Class 1: 3.1-4.0 Class 2: 4.1-5.0 Class 3: 5.1-6.0
Specific thermal capacity	c_p	Jkg ⁻¹ K ⁻¹	720	800
Thermal conductivity	λ	Wm ⁻¹ K ⁻¹	1	1
Average refractive index within the visible spectrum	n	-	1.52	1.5
Emissivity	ε	-	0.837	0.837

3 State of art on glass beam systems

3.1 Structural behaviour

3.1.1 Reinforced Glass Beams

One way to obtain the desired ductility is by adding a steel section at the bottom (or at the tensile zone) of the beam. This steel has the role to avoid the crack opening, i.e., the cracks still appear but it's much more difficult to get to a critical stage. Thanks to this phenomenon the cracks will not run over the full height of the beam. Such composite section is capable to generate significant post-breakage resistance. (Louter, 2011) (Figure 3.1)

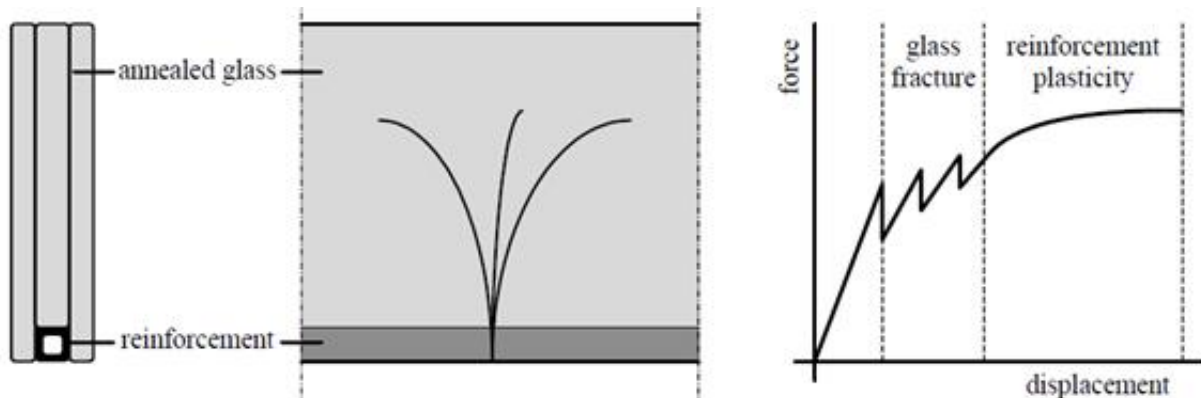


Figure 3.1 – Reinforced glass beam cross section and its Ductility (Louter, 2011)

3.1.2 Post-tensioned Glass Beams

With the reinforced glass beam concept, glass beams have now the particularity of bearing load after the cracking of the glass, i.e., it has now a ductile behaviour such as steel or concrete but has also the advantage of transparency. Despite this, its strength is still lower than that of any of the others. That is why engineers are now developing new ways to improve the strength of glass beams. One method found is by pre-tensioning the beam.

Figure 3.2 illustrates the favourable stress state induced by the pre-stress system. The crack initiation and propagation are prevented in compression (see 2.3) so by inducing the pre-stress field it leads the glass to a more advantageous situation with a longer region subjected to compression instead of tension.

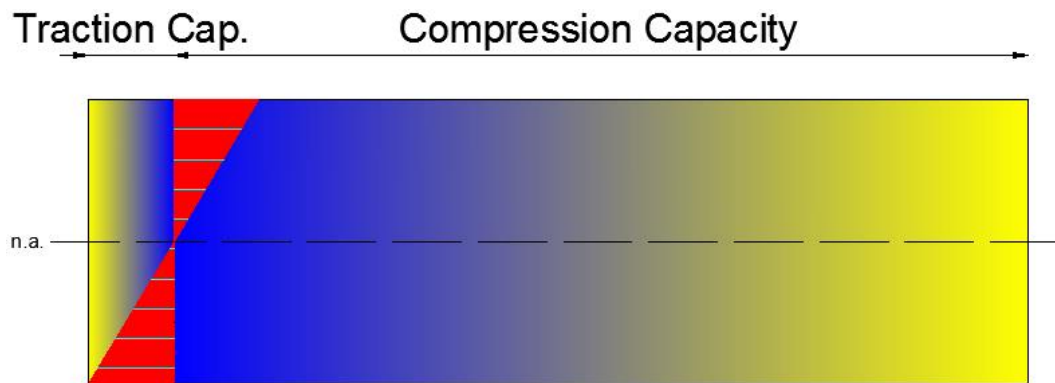


Figure 3.2 – Traction capacity vs Compression Capacity (Adapted from Diaz et al., 2011)

It was due to this fact that the post-tensioned glass beam appeared. By adding a compression Stress previous to the load the maximum capacity of the beam is reached to a greater load value.

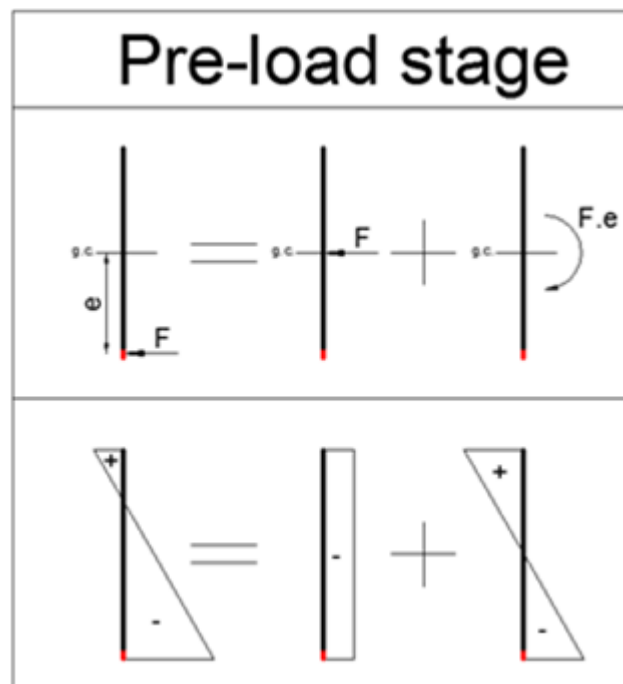


Figure 3.3 – Internal forces of the cross section before loading

3.1.3 Tempered Glass Beams vs Laminated Glass Beams

It has already been said that annealed laminated glass has a better post-breakage behaviour than that of tempered laminated glass (see 2.2.2). Regarding (laminated) glass beams a study was performed in Louter, 2011 and the conclusions were similar. Tempered glass beams shatter to a higher load but the remaining load carrying capacity is minimal when compared to laminated glass beams. (Louter, 2011) The Figure 3.4 tries to illustrate this phenomenon:

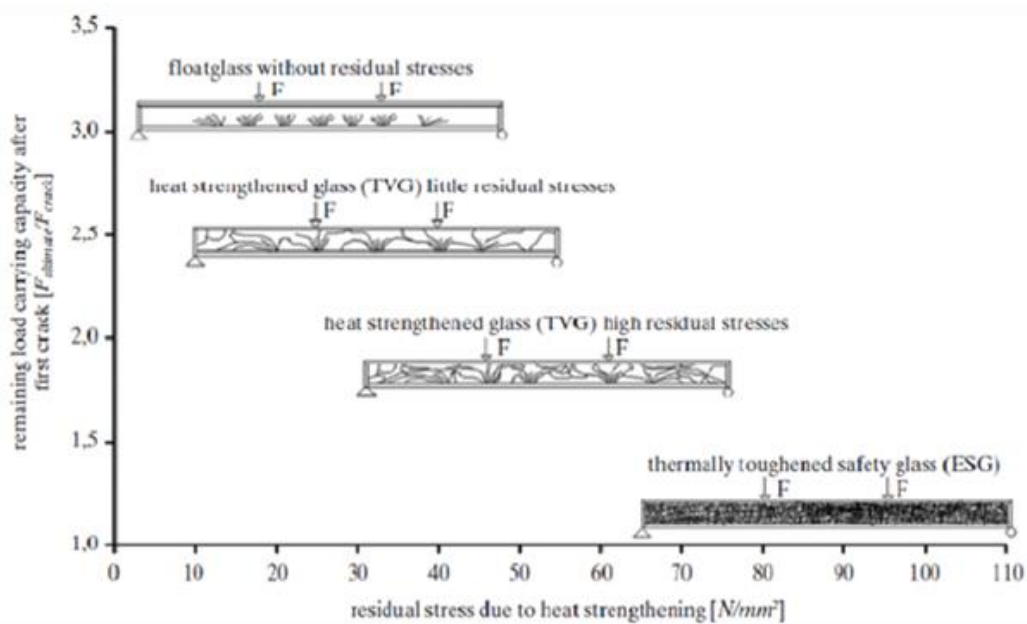


Figure 3.4 – Remaining load carrying capacity after first crack between annealed and tempered glass (Louter, 2011)

3.2 Overview of similar post-tensioned beams

In 2004 a post-tensioned glass beam prototype had already been tested by Louter (Louter, 2004). Such beam had a T-section. Composed by 3 layers of segmented annealed glass. A curved stainless steel section has been integrated in the web of the beam. Through this hollow section a $\phi 7$ high strength steel tendon was fed and tensioned at the beam ends. The pre-tensioning creates a compression field at the beam and, due to its curvature provides an upwards lift and additional resistance to the beam. From the results of this study it was concluded that the concept of post-tensioning an annealed glass beam is feasible and highly beneficial, however the explosive failure poses possible risks for building applications.

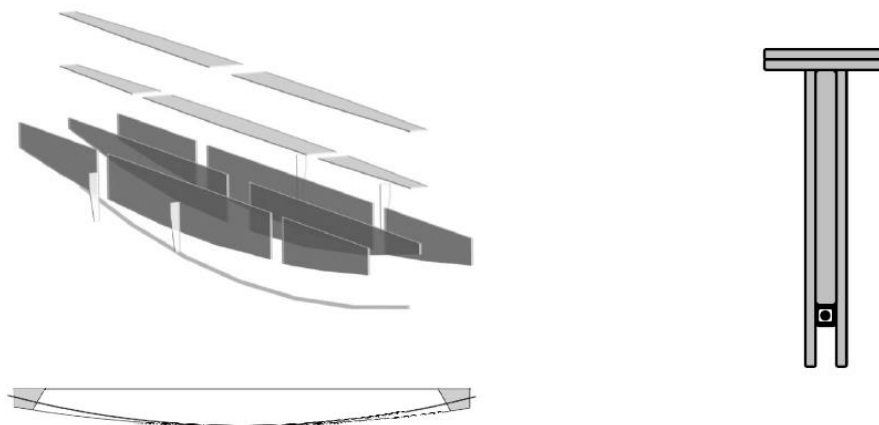


Figure 3.5 – T-section beam layout [left] and cross section [right] (Louter, 2008)

In (Froli & Lani, 2010) hybrid pre-stressed steel-glass beams are investigated. (Figure 3.6) The beam encompasses triangular double-layer PVB-laminated chemically tempered glass, stainless steel knots and steel tension cables. In the system the steels provides a ductile failure behaviour to the whole beam. In this works it was concluded that, different values of post-tensioning influence just the service of deformability of the beam but not its ultimate load.



Figure 3.6 – Hybrid pre-stressed steel-glass beam (Froli & Lani, 2010)

In (Jordão et al., 2014) a laminated glass beam reinforced with pre-stressed cables is numerically studied. The purpose of this paper was to establish a finite element model of the beam in which a parameter study was done regarding the choice of the element, the mesh dimensions, the choice of the feature used to model the lamination. Then benchmarking with experimental results and comparison was done to test the quality of the numerical model dealing with instability issues. A parametrical study regarding the optimal position of the cable was also done. (The main conclusions for this thesis were that S4 elements and 8 element along the beam's height lead to the best compromise between accuracy and time and the composite section formulation leads to equivalent contact formulation so it's better given the simplicity.

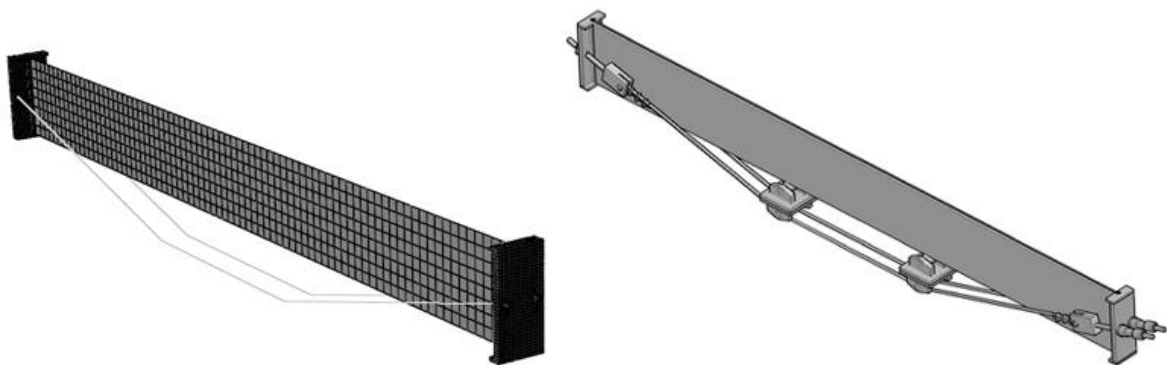


Figure 3.7 – Laminated glass beam reinforced with pre-stressed cables (Jordão et al., 2014)

In (Weller & Engelmann, 2014) a studied is performed to assess the deformation of the beam during post-tensioning. These deformations occur derived from imperfections. Due to this offset from the theoretical perfect state the applied axial force from post-tensioning will induce torsion and bending moments. During the experiments an imperfection of $L/1000$ was used. 4 layouts were studied. (Figure 3.8 and Figure 3.9) By analysing Figure 3.10 the out-of-plane displacement did not exceed $L/1000$. Thus, it's concluded that this layout indeed works during post-tensioning.

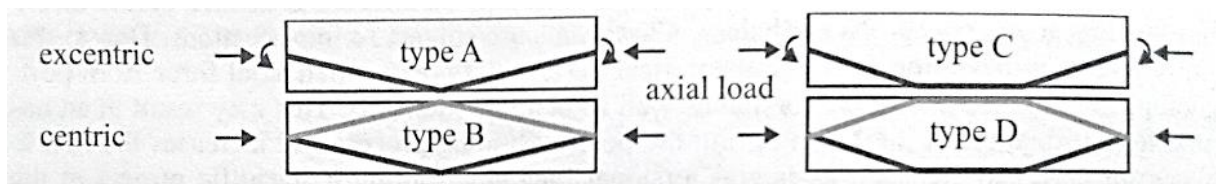


Figure 3.8 – 4 types studied in (Weller & Engelmann, 2014)

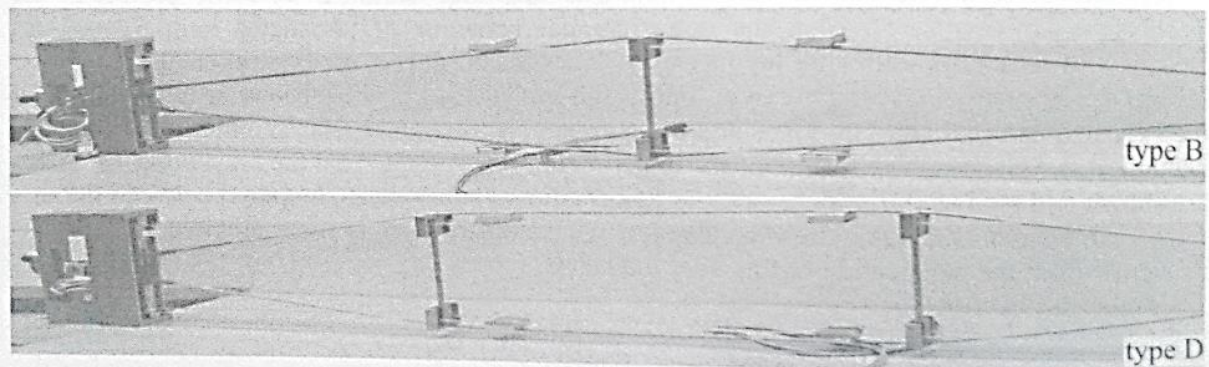


Figure 3.9 – Layout of the type B and type D beams (Weller & Engelmann, 2014)

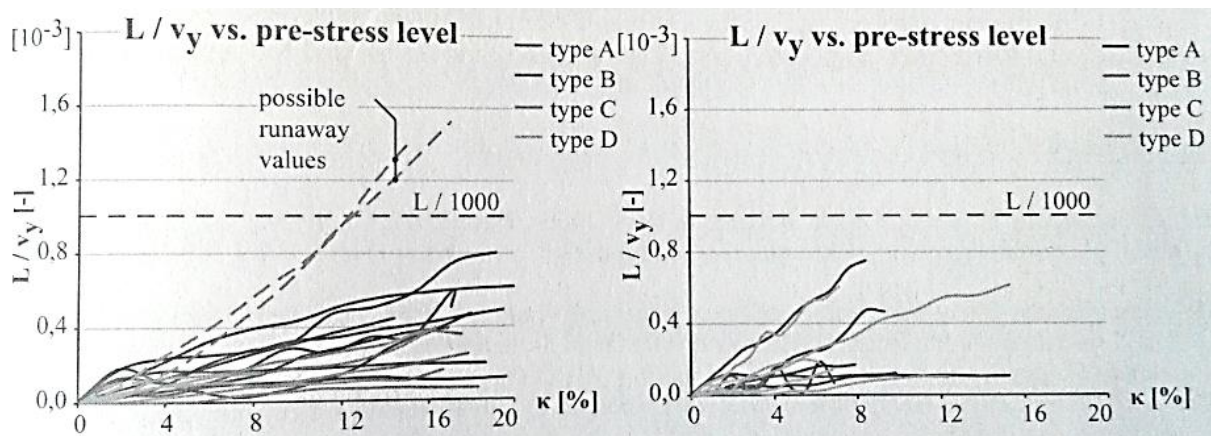


Figure 3.10 – Out of plane displacement (Weller & Engelmann, 2014)

In (Louter, 2013) a different post-tensioned systems were tested. (Figure 3.11) From the results it was concluded that these post-tensioned beams are feasible concepts in which the residual load-carrying capacity increased significantly, as well as the initial failure strength. Figure 3.12 shows the advantage of the post-tensioned glass beams when compared to beam only made with annealed glass.

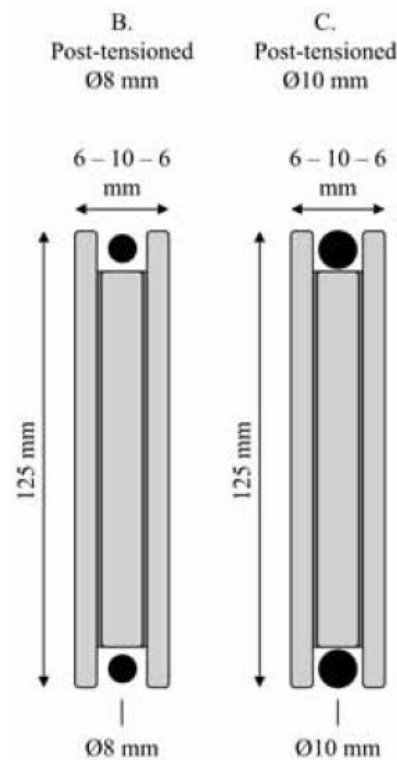


Figure 3.11 – Post-tensioned beams tested in (Louter, 2013)

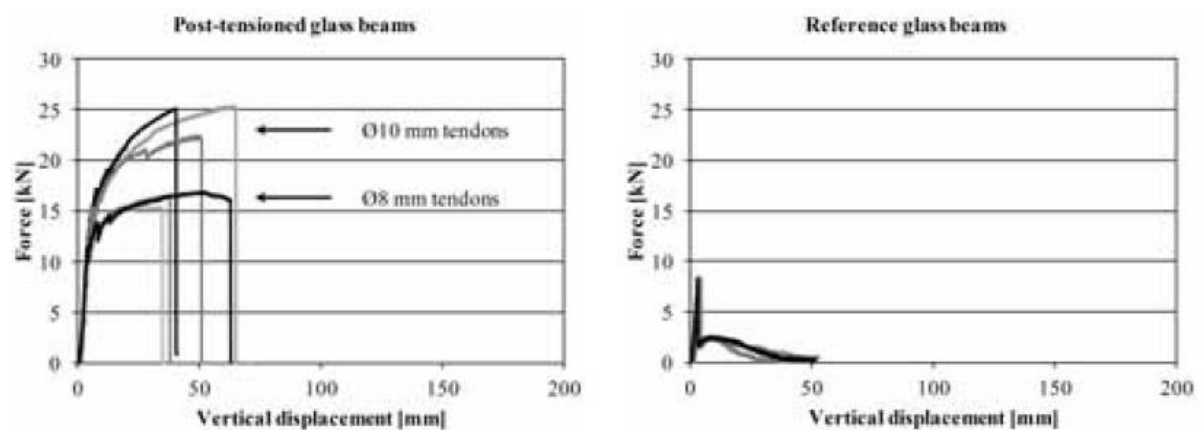


Figure 3.12 – Structural Behaviour of two glass beams. (Louter, 2013)

To follow (Froli & Lani, 2010) work, (Froli & Mamone, 2014) improve the length of the beam and develop now a 12m segmented glass beam. This beam is also composed by triangular and rectangular laminated glass panels assembled together by means of post-tensioned bars only. An experimental quasi-static cyclic test was performed experimentally and numerically. In Figure 3.13 it can be concluded that the model predicts well the yielding initiation in the lower bars, it overestimates the stiffness of the whole beam and its ultimate load-bearing model.

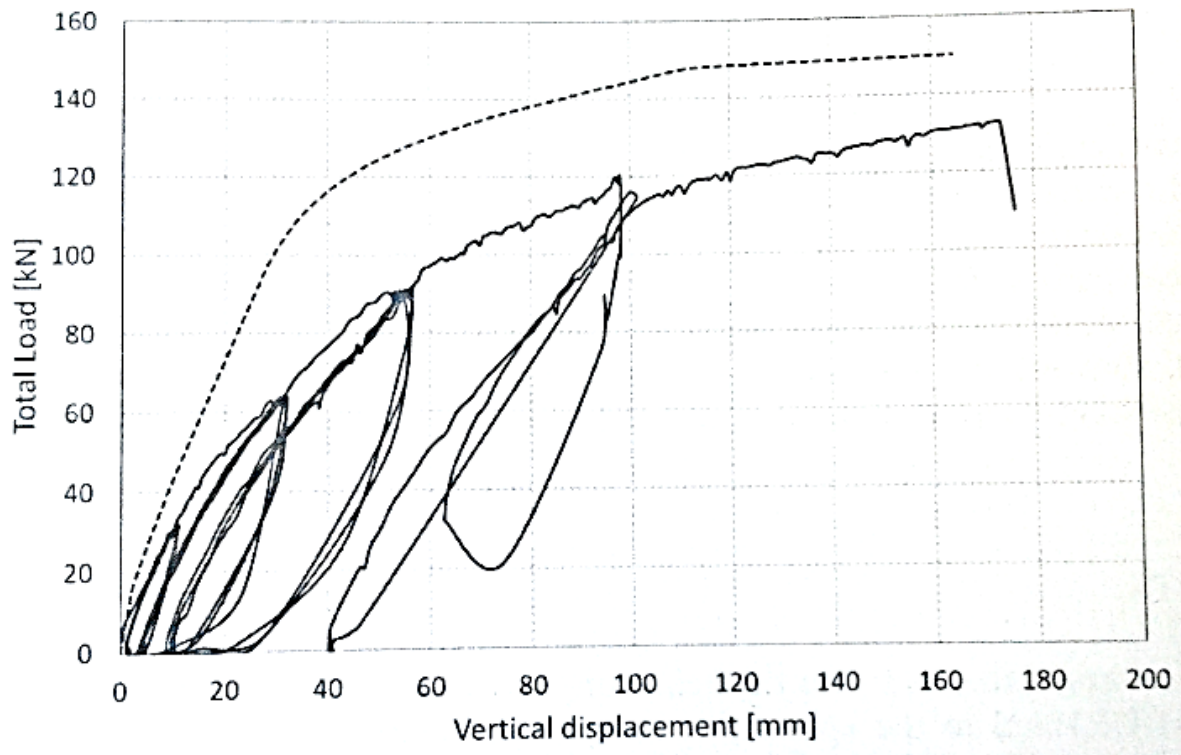


Figure 3.13 – Force vs Displacement plot (Froli & Mamone, 2014)

4 Experimental Analysis

4.1 Introduction

The experimental work and corresponding results presented in this chapter belong to the ongoing PhD thesis of Eng. MSc Jagoda Cupac. The referred thesis is being developed at École Polytechnique Fédéral de Lausanne (EPFL), under the supervision of Prof. Dr. Jean-Paul Lebet and under the co-supervision of Dr. Eng. Christian Louter. The experimental campaign was developed at the Laboratoire de la construction métallique (ICOM), EPFL. Eng. MSc Jagoda Cupac and her supervisors kindly authorized the use of the experimental data for the sole purpose of calibration of the FEM developed in the current thesis.

The purpose of the experimental tests is to characterize the behaviour of triple-laminated glass beam reinforced with a stainless steel strip at the bottom. In some tests the steel strip was post-tensioned.

The details of the experimental tests are summarised in Table 4.1 in which h_g , h_a , h_s , t_i , t_s , t_a and t_g stand for height of the glass, width of the adhesive, width of the steel, thickness of the interlayer, thickness of the steel, thickness of the adhesive and thickness of the glass, respectively.

Table 4.1 – Experimental study

Experiment	1st Exp NoPS	1st Exp PS	2nd Exp PS	2nd Exp NoPS	3rd Exp PS	3rd Exp NoPS
Date	14-03-14	31-03-14	13-05-14	14-05-14	16-05-14	19-05-14
h_g	122 mm	122 mm	122 mm	122 mm	122 mm	122 mm
h_a	1.5 mm	1.5 mm	1.5 mm	1.5 mm	1.5 mm	1.5 mm
h_s	25 mm	25 mm	25 mm	25 mm	25 mm	25 mm
t_i	(1.52x2) mm	(1.52x2) mm	(1.52x2) mm	(1.52x2) mm	(1.52x2) mm	(1.52x2) mm
t_s	3 mm	3 mm	3 mm	3 mm	3 mm	3 mm
t_a	1.5 mm	1.5 mm	1.5 mm	1.5 mm	1.5 mm	1.5 mm
t_g	(2x6+10) mm	(2x6+10) mm	(2x6+10) mm	(2x6+10) mm	(2x6+10) mm	(2x6+10) mm
Pre-Stress	Without	With	With	Without	With	Without

The PhD candidate Jagoda Cupac from EPFL is now studying the application of post-tensioned glass beams with a reinforcement at the bottom of the beam. The stainless steel will be pre-tensioned, creating an initial compressive stress where, when loaded, will be the maximum tensile stresses. Therefore, it can bear some more load before it cracks.

4.2 Layout and instrumentation

The layout corresponds to a 4PB arrangement, with the geometry shown in Figure 4.1. The details of the cross-section may be found in Figure 4.2. The out of plane displacement is prevented at the supports.

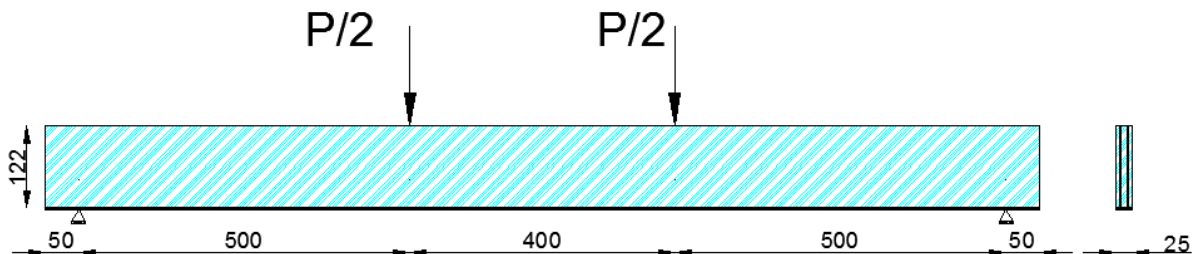


Figure 4.1 – Structural Model of the beam

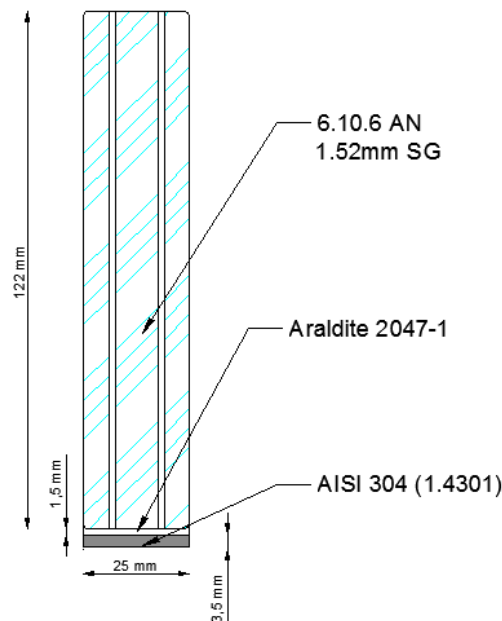


Figure 4.2 – Cross-section details

The instrumentation corresponds to a deflectometer at mid span, and the applied force to the beam was measured by the test machine load cell. The pretension force in the steel reinforcement was measured by load cells during the pre-tension and curing of the adhesive.

Since the weight of the whole beam is much lower than the actual load and to simplify the numerical modelling, such force wasn't considered.

4.3 Materials

4.3.1 Glass

The beam is made of annealed glass due to the reasons shown in 3.1.3. Although the failure stress is higher, tempered glass has a worst structural behaviour once the cracking occurs.

The failure stress of glass is a value with high dispersion. It doesn't only depend on the processing but also depends on the ambient conditions. Thus, and despite the common value suggested in the bibliography of 45MPa , the strength of the beam was calculated analytically according to the experimental data.

The first crack is clearly visible in the Force-Displacement Curve, corresponding to the first "jump" in the graphic. With that piece of information the exact load that caused the first crack can be pinpointed. Equation (3.1) was used to calculate the tension of the beam when the first crack appeared was the following, yielding the value of 46 MPa.

$$\sigma = -\frac{N}{A} + \frac{-M_{PS} + M_{Load}}{\left(\frac{I}{v}\right)} \quad (3.1)$$

Where N , A , M_{PS} , M_{Load} , I and v stand for Pre-Stress, Cross sectional area of the whole beam, equivalent moment due the pre-stress, moment due the loading in the moment of the first crack, moment of inertia in its strong axis and distance from the geometrical centre of the beam to the top of the glass, respectively.

4.3.2 Stainless Steel

Stainless steels are a large family of iron-chromium based alloys. By adding chromium the steel is now corrosion resistant in a variety of environments. Stainless Steel was used over usual steel given the exposure that the steel has in the whole beam. That way, in normal conditions, a stainless material can be assured through its living time. (Louter, 2008)

Between the stainless steels there are the austenitic stainless steels class, in which AISI 304 is amongst. AISI 304 was chosen for this research given the fact that, in terms of total industrial usage, it's the most commonly used. (Louter, 2008)

The nominal curve for stainless steel grade AISI304 (1.4301) is in Figure 4.3.

Table 4.2 – Nominal values for AISI 304 (adapted from Louter, 2011)

Density	ρ	kg/dm ³	7.9
Modulus of Elasticity at 20°C	E	GPa	200
Yield Strength 0.2% proof	$f_{y,0.2\%}$	MPa	210-230
Ultimate tensile strength	f_t	MPa	520-750
Elongation at fracture	ε_r	%	45

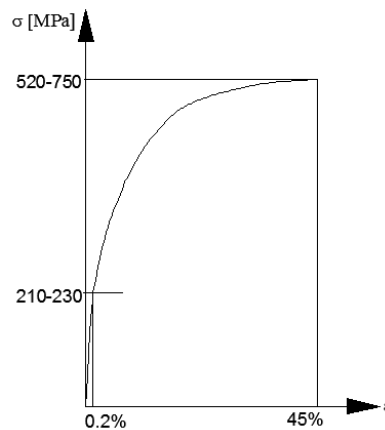


Figure 4.3 – Nominal curve for AISI 304

4.3.3 Adhesive

The adhesive used is Araldite 2047, which corresponds to an acrylic with a shear and tensile strength of 20 MPa and 13-15 MPa, respectively and an elongation at break of 13-15%. (Huntsman, 2013) This adhesive was chosen on the basis of previous research by (Belis et al., 2011) (Nhamoinesu and Overend, 2012). Figure 4.4 shows the different behaviour between the chosen adhesive and the other standard adhesives. It was applied with a thickness of 1.5mm.

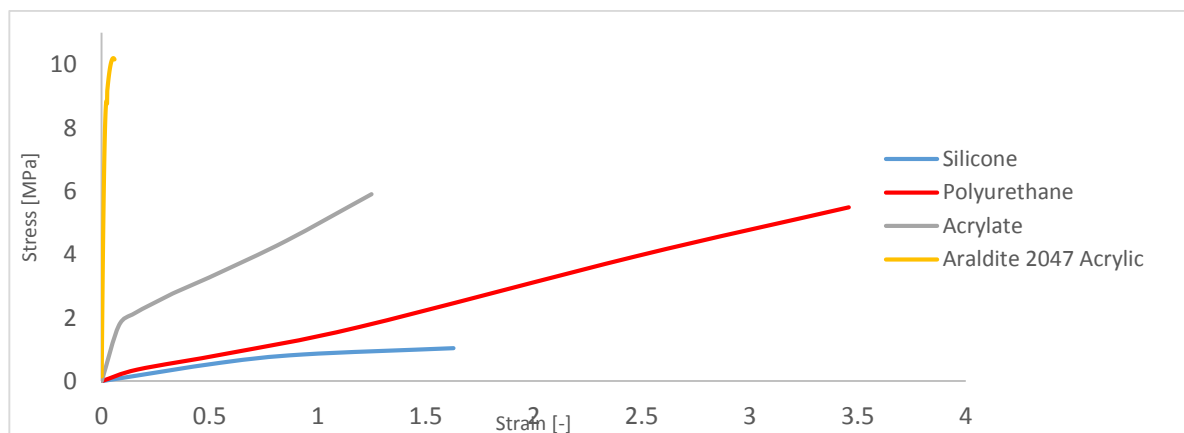


Figure 4.4 – Structural behavior of the adhesive according to (Nhamoinesu and Overend, 2012)

4.3.4 Interlayer material

The interlayer material is Sentryglas Plus® (SGP). Each layer is 1.52mm thick. The elastic properties of the SGP are shown in Figure 4.5.

		Load Duration						
Young's Modulus E (MPa)		1 s	3s	1 min	1 hr	1 day	1 mo	10 yrs
Temperature	10 °C	692	681	651	597	553	499	448
	20 °C	628	612	567	493	428	330	256
	24 °C	581	561	505	416	327	217	129
	30 °C	442	413	324	178	148	34.7	15.9
	40 °C	228	187	91.6	27.8	13.6	9.86	8.84
	50 °C	108	78.8	33.8	12.6	8.45	6.54	6
	60 °C	35.3	24.5	10.9	5.1	3.87	3.24	2.91
	70 °C	11.3	8.78	5.64	2.52	1.77	1.44	1.35
	80 °C	4.65	3.96	2.49	0.96	0.75	0.63	0.54

		Load Duration						
Shear Modulus G (MPa)		1 s	3s	1 min	1 hr	1 day	1 mo	10 yrs
Temperature	10 °C	240	236	225	206	190	171	153
	20 °C	217	211	195	169	146	112	86.6
	24 °C	200	193	173	142	111	73.2	43.3
	30 °C	151	141	110	59.9	49.7	11.6	5.31
	40 °C	77.0	63.0	30.7	9.28	4.54	3.29	2.95
	50 °C	36.2	26.4	11.3	4.20	2.82	2.18	2.00
	60 °C	11.8	8.18	3.64	1.70	1.29	1.08	0.97
	70 °C	3.77	2.93	1.88	0.84	0.059	0.48	0.45
	80 °C	1.55	1.32	0.83	0.32	0.25	0.21	0.18

		Load Duration						
Poisson Ratio ν		1 s	3s	1 min	1 hr	1 day	1 mo	10 yrs
Temperature	10 °C	0.442	0.443	0.446	0.45	0.454	0.458	0.463
	20 °C	0.448	0.449	0.453	0.459	0.464	0.473	0.479
	24 °C	0.452	0.453	0.458	0.465	0.473	0.482	0.489
	30 °C	0.463	0.466	0.473	0.485	0.488	0.497	0.499
	40 °C	0.481	0.484	0.492	0.498	0.499	0.499	0.499
	50 °C	0.491	0.493	0.497	0.499	0.499	0.5	0.5
	60 °C	0.497	0.498	0.499	0.5	0.5	0.5	0.5
	70 °C	0.499	0.499	0.5	0.5	0.5	0.5	0.5
	80 °C	0.5	0.5	0.5	0.5	0.5	0.5	0.5

Figure 4.5 - Properties of SGP depending on time of load and temperature (Stelzer, 2010)

4.4 Loading

6 tests were performed, 3 with and 3 without Pre-stress. For each series 3 speeds were considered. 1 mm/min, 2 mm/min and 5 mm/min.

In the cases with PS, it was applied an initial step:

1. The stainless steel strip is tensioned with a force of 15 kN leading to a stress of 200 MPa on the steel, which was near the normative yield stress value (Ruukii, 2014).
2. The adhesive is applied to the steel strip and to the beam.
3. When the adhesive is cured, the PS supports are released and the PS force is transferred to the glass.
4. The beam is tested with the vertical force.

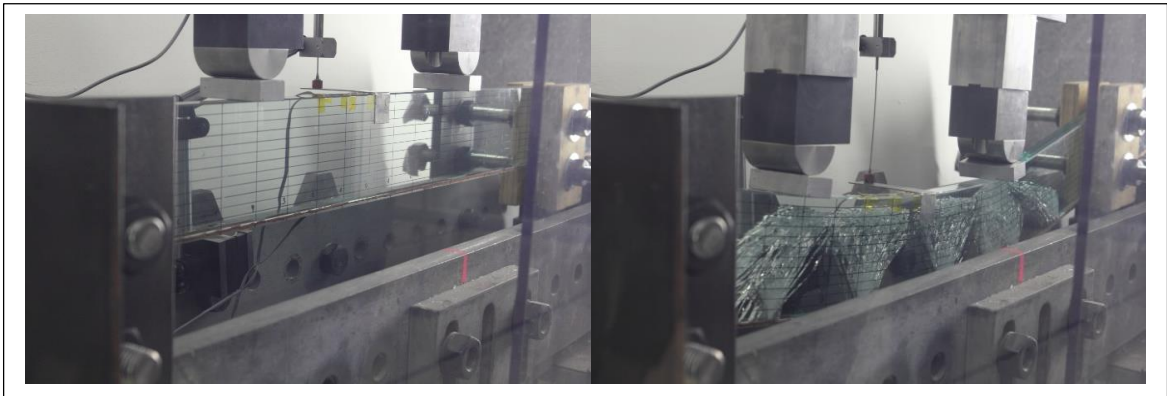


Figure 4.6 - Unloaded beam (left), Loaded Beam (Right)

4.5 Structural Model

The propagation of the cracks only occur in traction, and since there's the steel to hold the traction after the cracking, the top of the beam is always compressed. Therefore, the crack propagation stops as shown in Figure 4.6. (Louter, 2011) This concept may be understood in by analysing Figure 4.7:

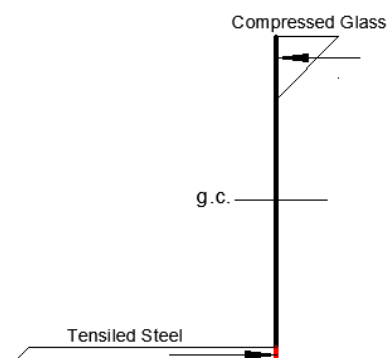


Figure 4.7 - Stress distribution after the cracking

The internal forces due the Pre-Stress step are represented in Figure 4.8 and the internal forces due the loading step are represented in Figure 4.9.

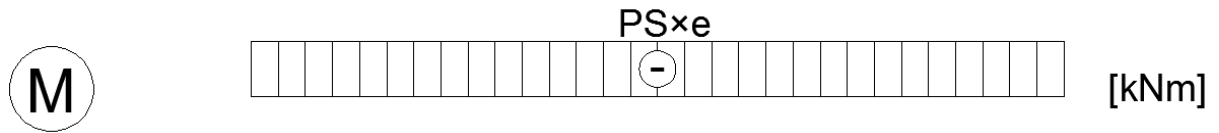


Figure 4.8 – Internal forces due to the Pre-Stress step

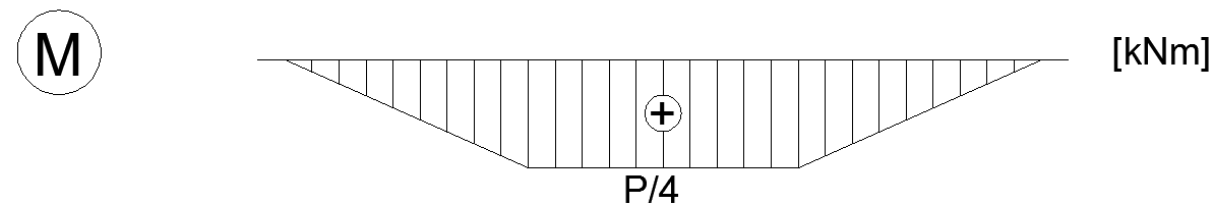
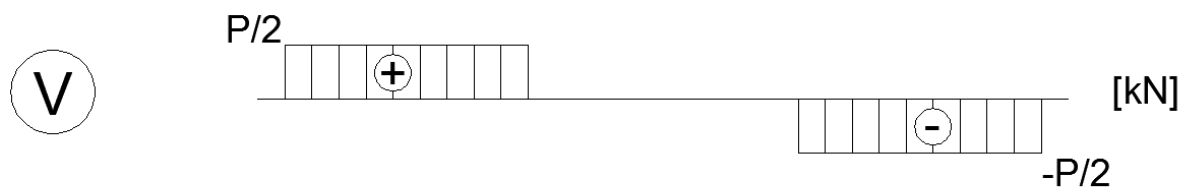


Figure 4.9 – Internal forces due to the Loading Step

4.6 Results

The results for the reinforced beam and reinforced post-tensioned beams are depicted in Figure 4.10a) and Figure 4.10b), respectively. Figure 4.11 shows a comparison between the results of a reinforced and a post-tensioned beam.

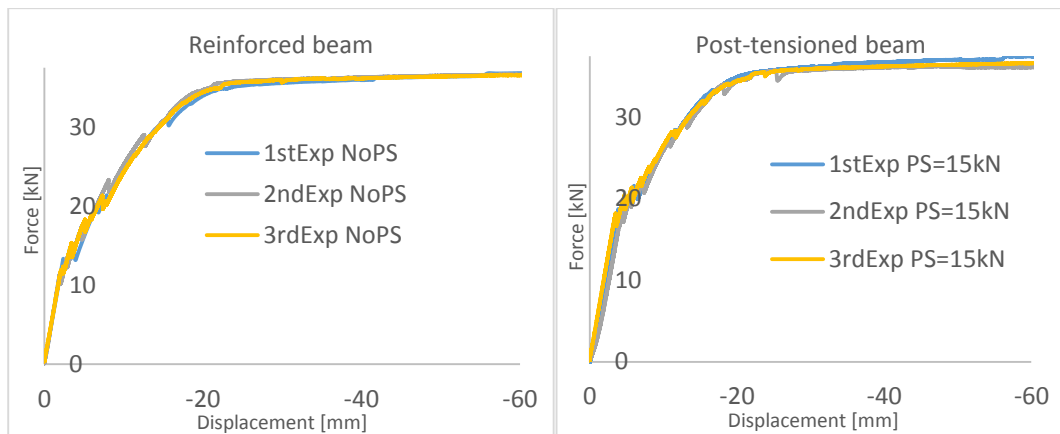


Figure 4.10 - Provided Data from Experiments in Reinforced Glass Beams (Left) and Post-tensioned Glass Beams (Right)

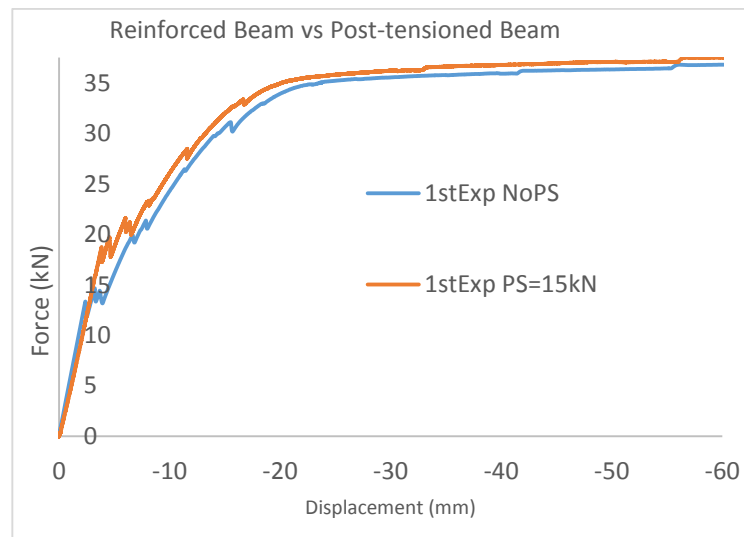


Figure 4.11 – Difference between the reinforced beam behavior and the post-tensioned beam behavior

From the results it can be concluded that the main advantage of the post-tensioned glass system is that the first crack appears for a higher load – it can be observed that for the reinforced glass beam and for the post-tensioned glass beam the first crack appears at approximately 13kN and 18kN, respectively. For higher loads the post-tensioned beam behaves similarly to the reinforced glass beams.

The reason for this is related with PS losses. In fact the pre-stress is applied on the steel that is transferred to the glass through the adhesive, but as the adhesive deforms the pre-stress decreases. This effect is increased when the cracks appear at the bottom of the glass. It then creates some debonding and instantaneous bending and so some more pre-stress is lost.

5 Numerical Analysis

The objective of the present chapter is the establishment of the numerical model. It is intended to reproduce the behaviour of the prototype used in the experimental campaign, so all the geometry layout and material properties will be reproduced. After calibration with the experimental results the numerical model will be used for a parametrical analysis aiming to completely characterize the behaviour of the structural model under study.

5.1 Structural model

The structural model corresponds to the experimental layout. In order to save time and since the setup was symmetrical, only half of the beam was considered in the numerical analysis. So 3 boundary conditions were assumed:

- Mid Span symmetry
- Simple supported blocking vertical displacement
- Simple supported blocking horizontal out-of-plane displacement



Figure 5.1 - Representation of the boundary conditions

5.2 Element type

The numerical analysis was done with shell elements. Nevertheless a comparison was established between the calculations of the model with Shell elements and the calculations of the model with 3D deformable elements and the difference was minimal as it can be shown in Table 5.1. This analysis was done in 2D elements without the Adhesive (2 parts), 2D elements with the adhesive included (3 parts) and 3D elements with the adhesive included (3 parts). To avoid calculating two steps in the Finite Element Analysis (FEA) software, these analysis were done on the reinforced glass beam. It was chosen homogeneous meshes with square/cubic elements for steel and adhesive and triangular/tetrahedral elements for glass. The results of this analysis are shown in Table 5.1. A mesh convergence study was performed (10mm, 5mm, 3mm, 2mm).

Table 5.1 – Analysis type and Mesh Study

REINFORCED GLASS BEAM	2D Analysis		2 Parts	Load = 6.665 kN= 13.3333/2
	Mesh Size	σ_{\max} In-Plane Principal	σ_{\min} In-Plane Principal	δ_{midspan}
	10 mm	47.69 MPa	-74.39 MPa	-2.48 mm
	5 mm	47.69 MPa	-80.12 MPa	-2.48 mm
	3 mm	47.69 MPa	-82.73 MPa	-2.48 mm
	2 mm	47.69 MPa	-82.29 MPa	-2.48 mm
	2D Analysis		3 Parts	Load = 6.665 kN= 13.3333/2
	Mesh Size	σ_{\max} In-Plane Principal	σ_{\min} In-Plane Principal	δ_{midspan}
	10 mm	45.41 MPa	-54.88 MPa	-2.43 mm
	5 mm	46.31 MPa	-64.19 MPa	-2.47 mm
	3 mm	46.68 MPa	-69.54 MPa	-2.49 mm
	2 mm	47.00 MPa	-74.34 MPa	-2.50 mm
	3D Analysis		3 Parts	Load = 6.665 kN= 13.3333/2
	Mesh Size	σ_{\max} In-Plane Principal	σ_{\min} In-Plane Principal	δ_{midspan}
	10 mm	43.50 MPa	-55.22 MPa	-2.57 mm
5 mm	45.49 MPa	-65.71 MPa	-2.55 mm	
3 mm	46.35 MPa	-70.59 MPa	-2.56 mm	
2 mm	46.75 MPa	-74.70 MPa	-2.49 mm	

It was observed that for the 2D simulation without the adhesive the stress was too high when compared with the analytical approach (see 4.3.1). It was also found that the difference of stresses between the 2D simulation and the 3D simulation aren't significant. Nevertheless, the calculation time for the 3D simulation was much higher than the calculation time for the 2D simulation. It was chosen the 2D model with the adhesive included (3 parts).

5.3 Explicit Analysis

Unlike steel, glass is brittle and when the strength of the material is reached it cracks instead of yielding. It was necessary to define properly the numerical assessment of the brittle cracking. In order to define the brittleness of the material it's necessary to define the crack initiation and the post-cracked behaviour of the glass.

Abaqus software offers two ways of performing the analysis – Standard/Implicit or Explicit. In a standard analysis - the implicit analysis - the integration operator matrix must be inverted and a set of nonlinear equilibrium equations must be solved at each time increment. In an explicit analysis displacements and velocities are calculated in terms of quantities that are known at the beginning of an increment; therefore, the global mass and stiffness matrices don't need to be formed and inverted, which means that each increment is less expensive than in a standard analysis. (Abaqus, 2012)

The explicit dynamics procedure has the advantage of being able to process large rotations and deformations and can be used to perform quasi-static analysis with complicated contact conditions. Unlike the Standard analysis, where the equilibrium must be validated, in the explicit analysis the calculations are based on Newton's Second law (Mashayekhi, 2013), since the explicit dynamics procedure solves every problem as a wave propagation problem:

$$\sum F = m \cdot a \quad (5.1)$$

Where F , m and a stand for force, mass and acceleration, respectively.

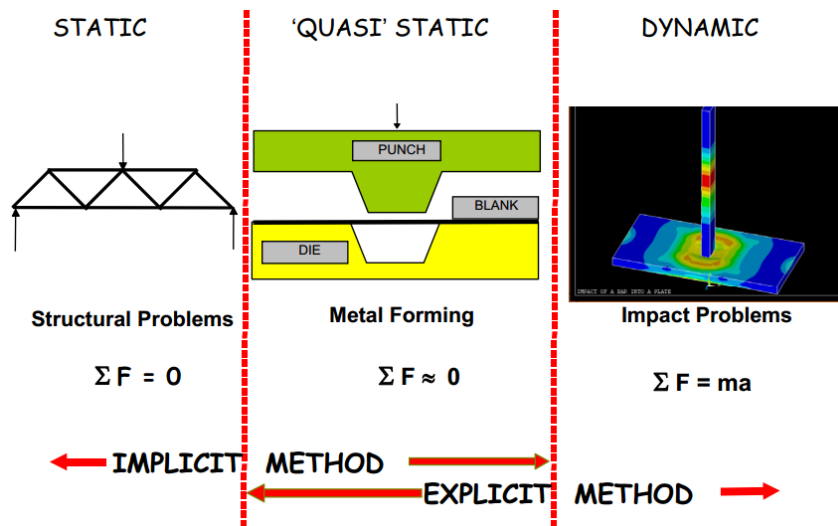


Figure 5.2 - Purposes of both analysis (Mashayekhi, 2013)

The explicit analysis is more suitable in order to simulate the quasi-static loading performed in the experiments due to the capability to use mass scaling to reduce the cost of the analysis and to have into account the brittleness of the material. Without such analysis the brittle cracking of the material could not be modelled. (Abaqus, 2012)

The calculations in an explicit analysis are done by stable time increments. That stable time increment, Δt , can be estimated by the following Equation (Abaqus, 2012)

$$\Delta t \approx \frac{L_{\min}}{c_d} \quad (5.2)$$

Where L_{\min} and c_d stand for smallest element dimension in the mesh and dilatational wave speed, respectively. The dilatational wave speed, c_d , may expressed as (Abaqus, 2012):

$$c_d = \sqrt{\frac{\hat{\lambda} + 2\hat{\mu}}{\rho}} \quad (5.3)$$

Where $\hat{\lambda}$ and $\hat{\mu}$ stand for Lamé's first parameter and Lamé's second parameter (also known as Shear Modulus), respectively. For application in Structural Engineering, in which materials are mainly isotropic and elastic it can be assumed that:

$$\hat{\lambda} = \lambda_0 = \frac{E\nu}{(1+\nu)(1-2\nu)} \quad (5.4)$$

$$\hat{\mu} = \mu_0 = \frac{E}{2(1+\nu)} \quad (5.5)$$

By these equations it can be deduced that the bigger the element, the bigger the stable time increment. The remaining parameters are properties of the material. The stable time increment will not remain constant in general, since element distortion will change the smallest element dimension during the analysis. These calculations were automatically done by the software. A fixed incrementation may be used but it is advised to use the automatic incrementation to avoid errors.

5.4 Quasi-Static Simulation

The beams were tested with low displacement ratios (see 4.4) so a quasi-static experiment may be assumed. A Quasi-static loading, by definition, refers to a slow loading in which the inertial effects can be negligible.

To have a really quasi-static simulation an amplitude was determined. (Figure 5.3). With such amplitude an increasing load is assured, i.e., in the beginning of the step the applied loading value is zero and in the end of the step the loading value is what it was determined.

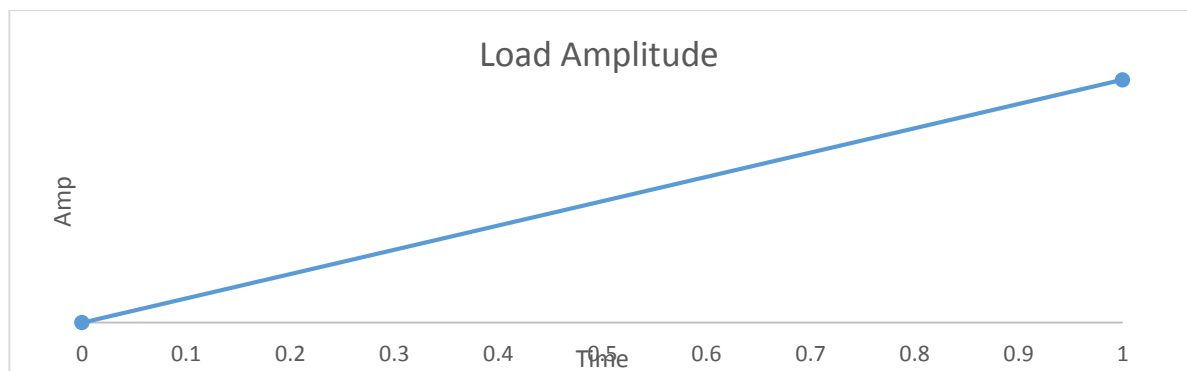


Figure 5.3 - Amplitude Imposed

5.5 Reducing the computational cost

As this is a complex and long analysis and the available time was extremely limited, reducing the computational cost was mandatory. In (Abaqus, 2012) 2 methods can be found to reduce the computational cost. These 2 ways are explained below:

5.5.1 Speeding up the simulation

One way to reduce the number of increments required, is to speed up the simulation compared to the time of the actual process, i.e., artificially reduce the time period of the event. By doing this 2 possible errors may occur:

- The increased inertia forces will change the predicted response, i.e., the problem may exhibit a wave propagation response.
- If the material behaviour is rate dependent the simulation will not be real.

5.5.2 Using Mass Scaling

The second way to reduce the number of increments is by artificially increasing the material density, ρ , by a factor of f^2 . Analysing the equations (5.2) and (5.3) it can be understood that by doing this the stable time increment increases f times.

Both of these methods were considered, due to the time limitation. The contact difficulties between the materials, the low density of some materials and the small displacement rates performed in the experiment made these analysis too difficult and so it is highly recommended that after the study of the parameters to input, an analysis with the adequate time and with a lower mass scale factor be carried.

After defining the amplitude, an analysis was carried to simulate an experiment in the reinforced glass beam. The first simulation was done with a total time of 1s which is the default definition of the software and with a mass scale factor of 1×10^6 . When plotted the reaction force at the support in function of the time period of the step the result depicted below as obtained:

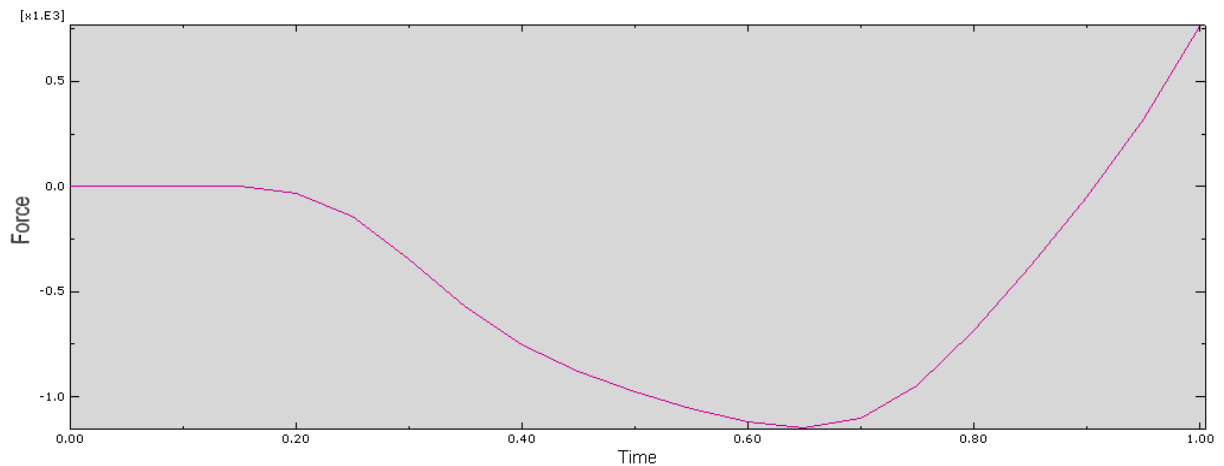


Figure 5.4- Reaction Force in function of Time when Step time was 1 computational second

It was immediately realized that the step must take more than 1 computational second to simulate the experiment. This inaccuracy happens due to the quick loading rate. The quick loading rate can be avoided by increasing the step time.

It was written before that the displacement ratio during the experiments had been 1mm/min, 2mm/min and 5mm/min. So, in order to get the most accurate simulation as possible, 1mm/min was assumed for the whole experiment.

For a displacement higher than 30mm the beam behaves as a plastic material, proving that the steel is the main material bearing load in the current state. As in this thesis the goal is to characterize the structural behaviour of the beam, i.e., the composite section, all the plots shown are until 30mm of displacement.

For a ratio of 1mm/min and in order to get 30mm of displacement it was necessary an analysis with 1800 computational seconds. Since this is unpractical and the resources were limited it was assumed 50 computational seconds. (Figure 5.5)

By the stable time increment, taken from (Bedon and Louter, 2014) and the adequate time calculated before, it is easy to get the required number of increments, n (Abaqus, 2012):

$$n = T/\Delta t = 1800/1.81 \times 10^{-7} = 9.94 \times 10^9 \quad (5.6)$$

Where T and Δt stand for time period and stable time increment, respectively.

This means that in order to get the real simulation almost *10 000* millions increments are needed. Abaqus explicit is able to process the calculations with two different precisions: the double precision and the single precision. The double precision executable makes the calculations with 64-bit word lengths instead of the usual 32-bit word lengths (single precision). By using the single precision it could be saved 20% to 30% of the CPU when compared to the double precision, however single precision tends to be inadequate in analysis that require a number of increments greater than 300 000. (Abaqus, 2012) Since it was done an explicit analysis and the number of increments required for each step was a significant number a double precision executable was used. (Bedon and Louter, 2014)

By assuming the *mass scale factor = 1 000 000* the *n* reduces *1 000* times, and by assuming a time period of *1s* the *n* reduces 1800 times. So *n'* increments were analysed:

$$n' = \frac{n}{\sqrt{f}} \times \frac{1}{1800} = \frac{n}{\sqrt{1000000}} \times \frac{1}{1800} \approx 5.56 \times 10^{-7} \cdot n \quad (5.7)$$

As this value is much lower than that of the experiment, an analysis with *50* computational seconds was tested. By doing this the number of increments was now:

$$n' = 2.8 \times 10^{-5} \cdot n \quad (5.8)$$

The same plot as before, but this time for 50 computational seconds may be find below:

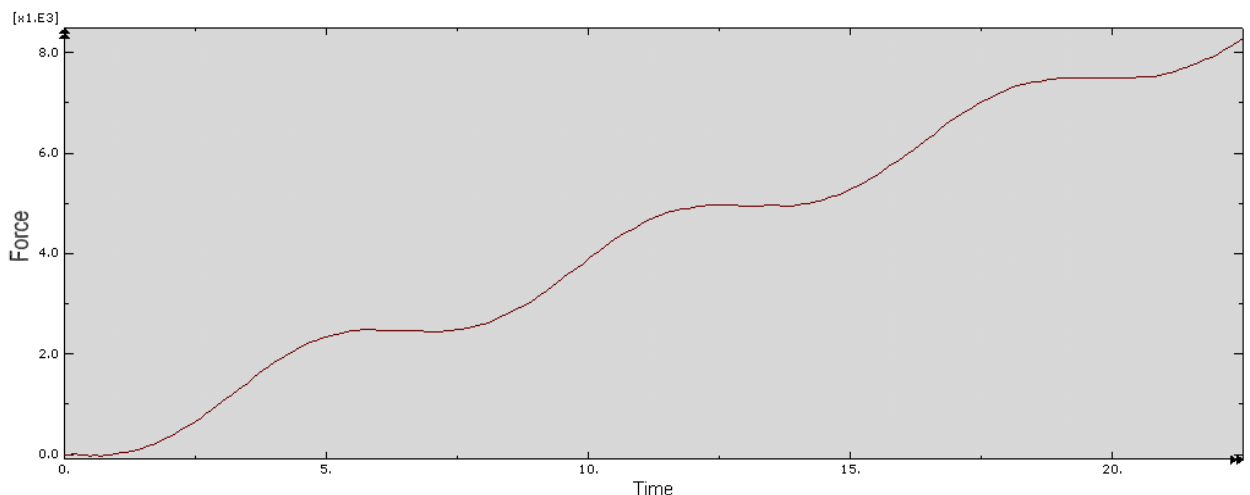


Figure 5.5 - Reaction Force in function of Time when Step time was 50 computational seconds

It is clear that, although the wave propagation response still exists, is much less significant than before. As it was said before, an analysis with a higher number of increments is highly recommended.

5.6 Influence of the interlayer in the numerical analysis

Almost all models for reinforced glass beams have been two-dimensional. By only using 2D elements the interlayers could not be taken into account in the numerical modelling. A study regarding the influence of the interlayer was done in (Louter and Nielsen, 2013) and it was concluded that a simulation is still highly dependent on the interlayers properties, particularly its Shear modulus, G , i.e., when the analysis is calculated without taking into account the adhesive, the plots force-displacement are slightly lower than that of the experiment. This fact is shown in Figure 5.6. For that reason the force-displacement plots given by the numerical calculations are expected to have a slightly smaller resistance than that of the experiments.

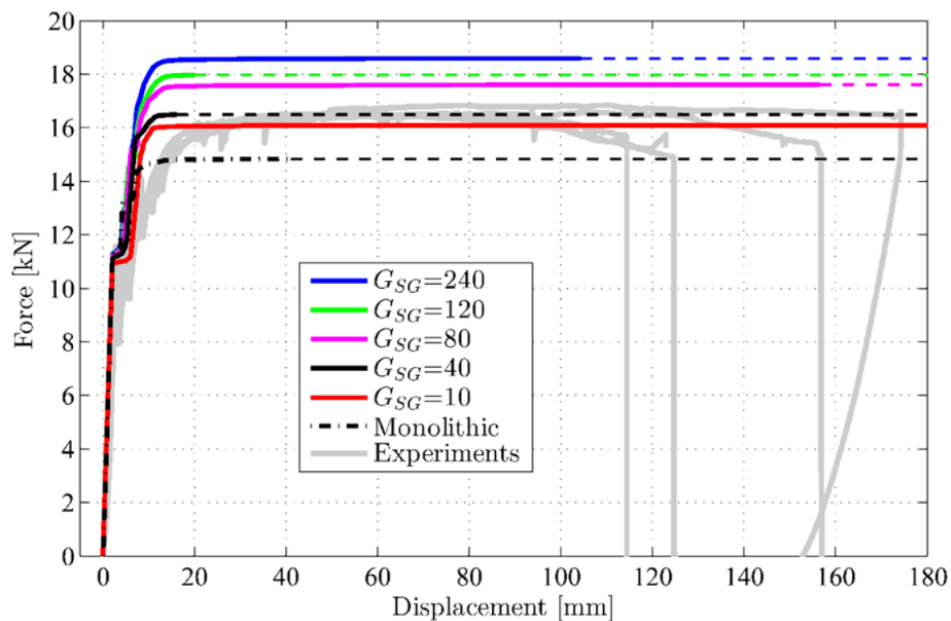


Figure 5.6 – The influence of the SGP in force-displacement curves (Louter et Nielsen, 2013)

5.7 Mesh

In (Beton and Louter, 2014) it is shown that a different mesh from bottom to the top of the beam is adequate, (1mm at the bottom and 5mm at the top particularly) and so the first numerical models including the brittle cracking were done with this fine mesh. Unfortunately, these models were shown to be too slow and too expensive for the limited time available, i.e., the Stable time increment, Δt , was 1.81×10^{-7} (Beton and Louter, 2014). After analysing Table 5.1, a homogeneous mesh of 3mm was chosen. By doing so, the stable time increment, Δt , dropped to approximately 5×10^{-7} , i.e. the analysis got 3 times faster as expected. (see 5.3)

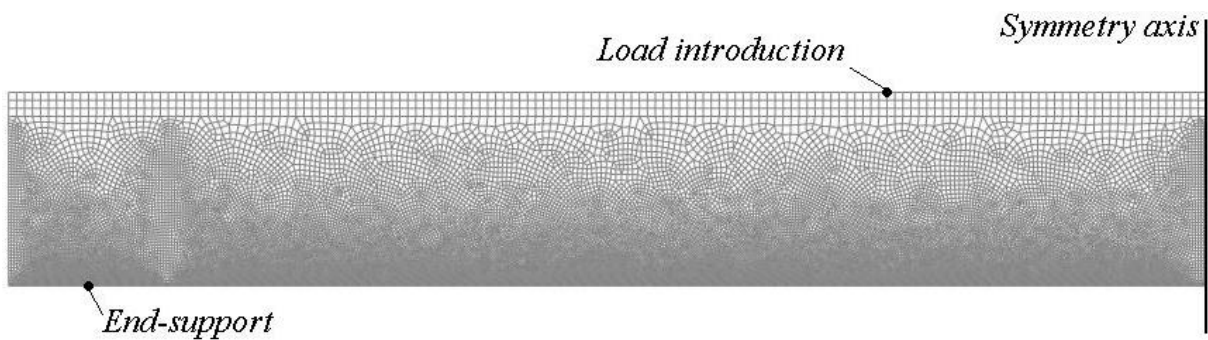


Figure 5.7 – Mesh pattern used in Bedon and Louter, 2014

As the size of each element is slightly bigger than the size practised in Bedon and Louter, 2014 it should be expected bigger irregularities on the graph of the numerical analysis done within this thesis. This happens because, since the elements are bigger, once it gets to the failure stress a relatively large portion of the beam is taken from the analysis when compared with the portion of the beam taken in Bedon and Louter, 2014.

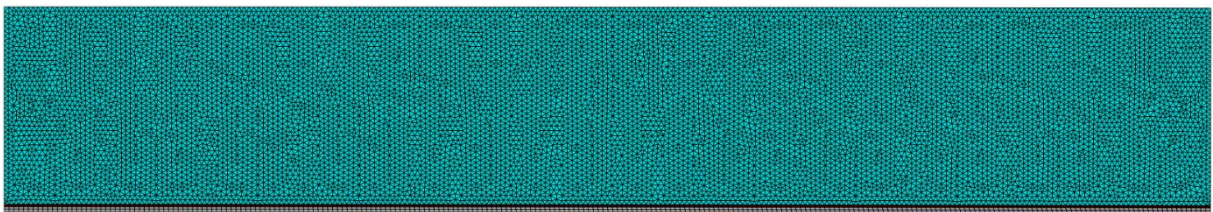


Figure 5.8 – Mesh pattern used within this study

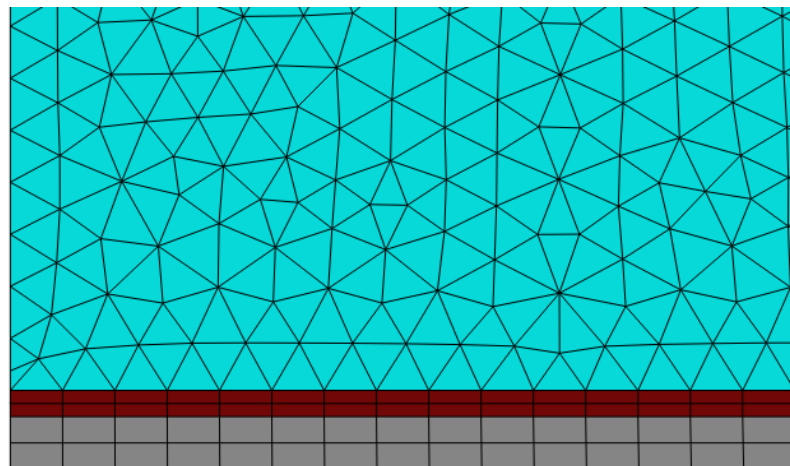


Figure 5.9 – Zoomed picture of the mesh used within the study at the bottom edge of the beam

The three different materials may be found in Figure 5.8 and in Figure 5.9. The blue, brown and silver colours corresponds to the glass elements, adhesive elements and steel elements, respectively.

5.8 Equivalent Cross Section

The real cross section (O in

Figure 5.10) encompasses three layers of annealed glass. Two of them with 6mm and another with 10mm. The interlayers were not modelled, so the beam could be modelled with Shell Elements.

In order to assess which one was the best to model the behaviour of the beam a comparison was established between the numerical and experimental results, for each equivalent cross section.

3 possibilities were considered. (A, B and C in

Figure 5.10). After analysing Figure 5.11 the possibility A was found to be the most suitable since its results are the ones closer to the experimental ones. In fact B has a lower strength B when compared to that of the experiment and C has a higher stiffness than that of the experiment.

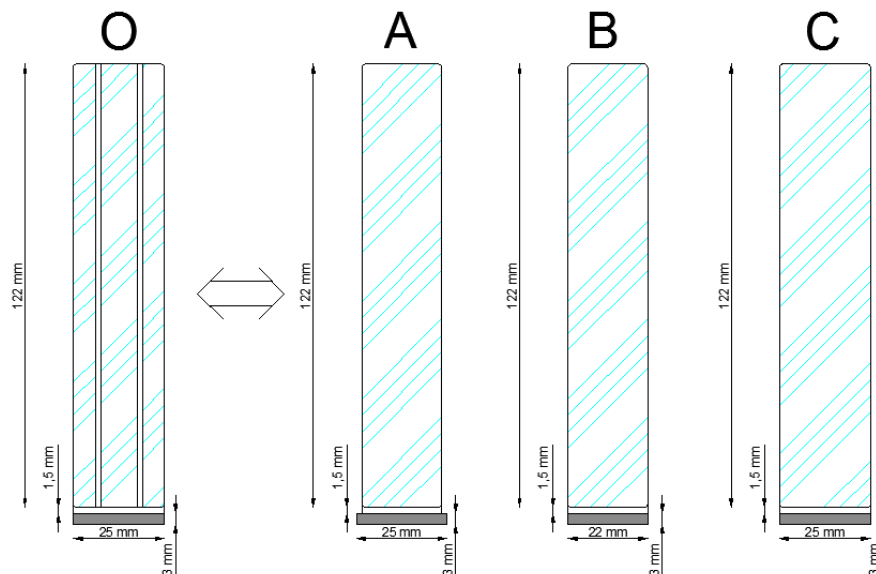


Figure 5.10 – Differences between the real [O] and the numerical cross sections [A, B and C]

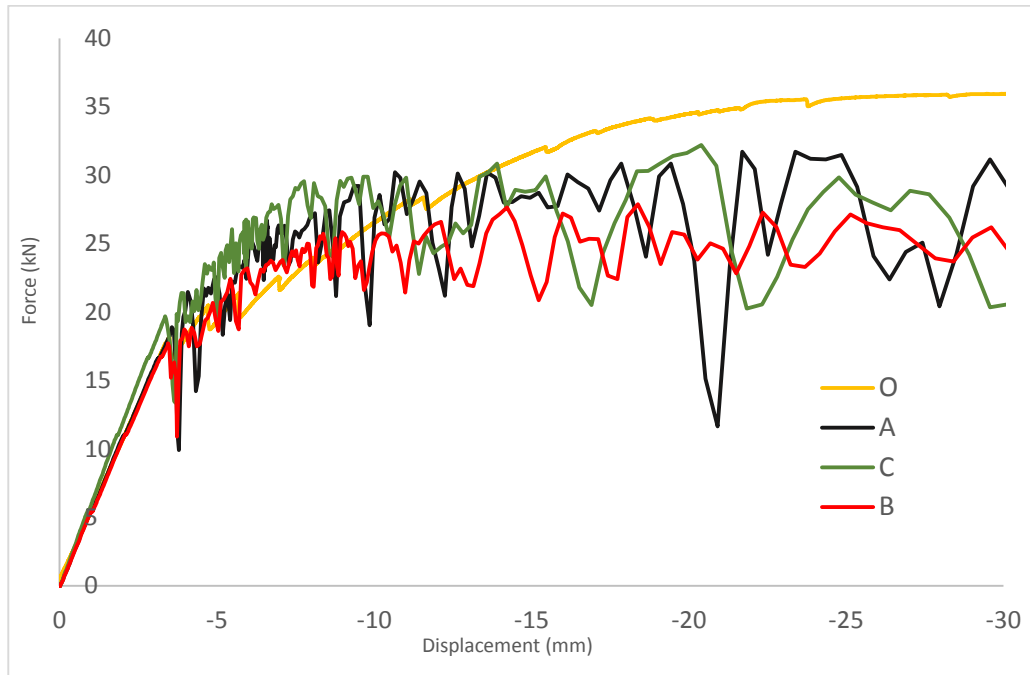


Figure 5.11 – Force-displacement curves from Experiment [O] and Numerical Analysis [A, B and C]

Although at first sight it appears an inaccurate simulation, taking into account what was mentioned in 5.6 and previous research, the plots shown in Figure 5.11 are indeed due to accurate simulations and show a good correspondence when comparing with the experimental results. The “jumps” shown in the plots correspond to elements deletion (see 5.11.3) and are also due to some dynamic response that isn’t inexistent in the model. (see 5.5)

5.9 Pre-Stress

The value of the pre-load was determined to be $15kN$ (see 4.4). As the used software doesn’t have the built-in function of *pre-stress* it was needed to calculate the equivalent variation of temperature, ΔT . The conductivity of the materials that were not to be pre-stressed was set to be zero in order to prevent heat transfer between the materials. With that variation it was possible to simulate the pre-stress. To calculate the ΔT , firstly it was needed to calculate the displacement, ΔL , in the steel due to the pre-stress of $15kN$.

$$\Delta L = \frac{NL}{E_s A_s} \quad (5.9)$$

Where N , L , E and A stand for determined pre-stress value, length of the beam, young’s modulus of the steel reinforcement and cross-sectional are of the steel reinforcement. The same displacement may be calculated due to a ΔT :

$$\Delta L = L \cdot \alpha \cdot \Delta T \quad (5.10)$$

Where α stands for coefficient of thermal expansion. Equating both of the equations we get:

$$\Delta T = \frac{N}{E \cdot A} \times \frac{1}{\alpha} = -65.7^\circ K \quad (5.11)$$

It was tried the force analogy (Figure 5.12), i.e., with the 15kN force on the edge of the beam but the stress distribution on the steel was found incorrect (Figure 5.13), i.e., different of what should be expected. By adding the pre-tensioning field it should be expected a bigger tension at half span of the beam and not at the edge. The stress distribution caused by the variation of temperature is the most accurate between these two (Figure 5.14). The axial force in Figure 5.14 doesn't reach the 15kN due to immediate pre-stress losses. These pre-stress losses are immediate and happen due to the bending.

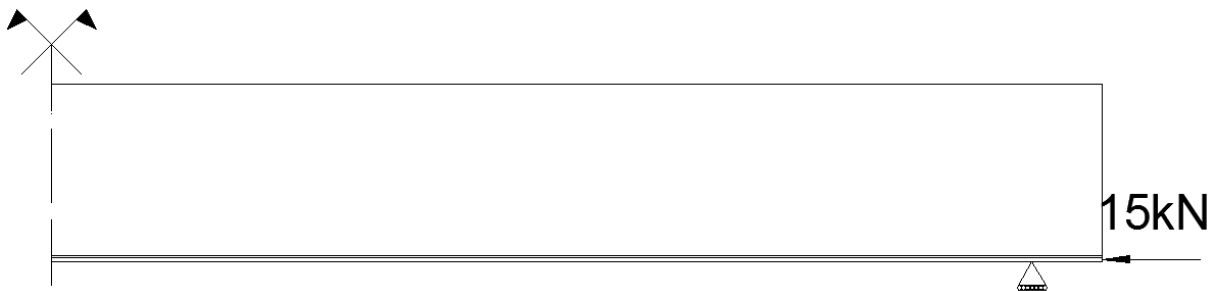


Figure 5.12 – Force analogy regarding the pre-stress

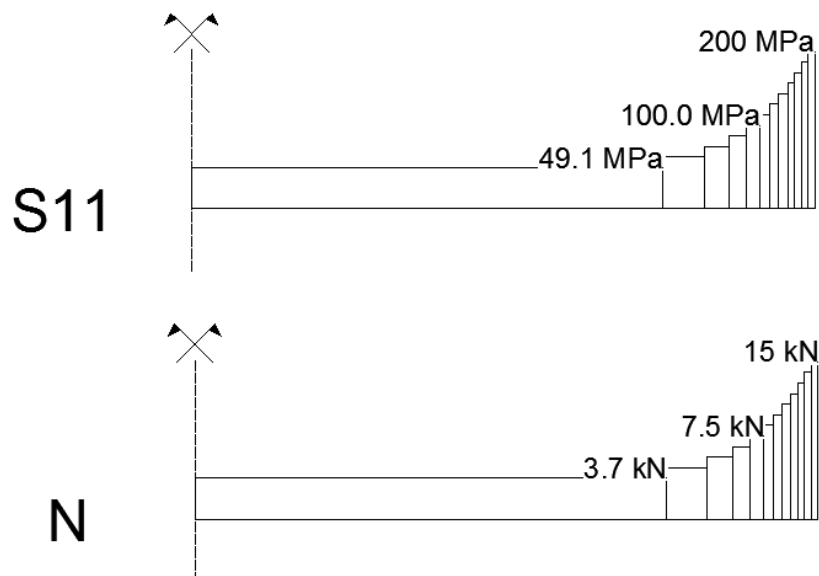


Figure 5.13 – Stress on the steel along its axis and its axial force due to the force analogy

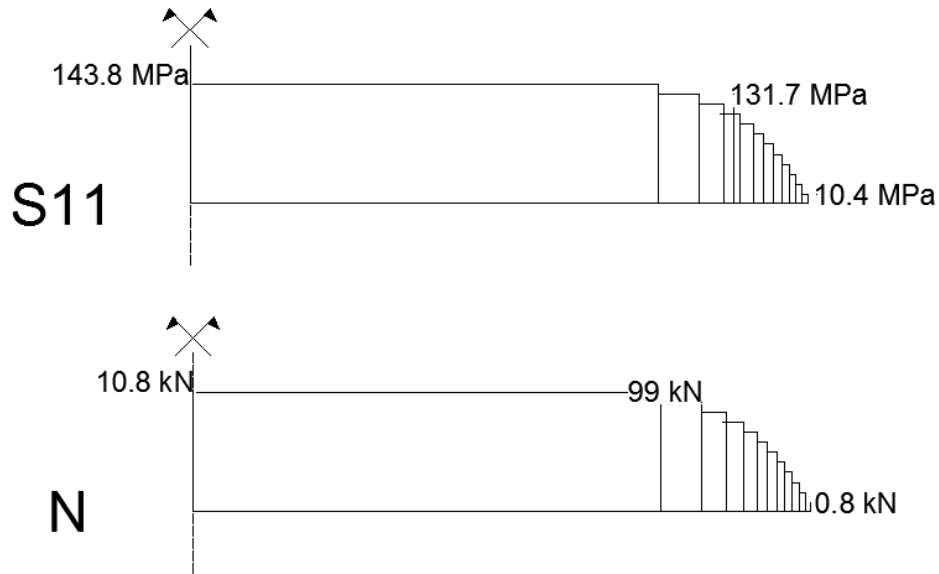


Figure 5.14 – Stress on the steel along its axis and its axial force due to the variation of temperature

To validate these calculations a comparison between the analytical approach and the numerical approach was done.

In order to use the analytical approach, the bending stiffness of the composite section, $EI_{composite}$, was calculated according to the following Equation (Louter, 2011):

$$EI_{composite} = E_{gl} \sum_{i=1}^n \left(I_{yy,i} \frac{E_i}{E_{gl}} + z_i^2 A_i \left(\frac{E_i}{E_{gl}} \right) \right) \quad (5.12)$$

Where E_{gl} stand for Young's modulus of glass (the main component in the section), E_i stand for Young's modulus of the considered component in the section, $I_{yy,i}$ stand for moment of inertia of the considered component, n stand for total number of components in the section, z_i stand for distance between the axis of the considered component and the neutral axis, i stand for considered component in the section and A_i stand for cross-sectional area of the considered element

The displacement was calculated according to the following equation (Dias da Silva, 2004):

$$\frac{1}{\rho} = \frac{M_{PS}}{EI_{composite}} \quad (5.13)$$

Where ρ and M_{PS} stand for bend radius and moment installed due the pre-stress, respectively.

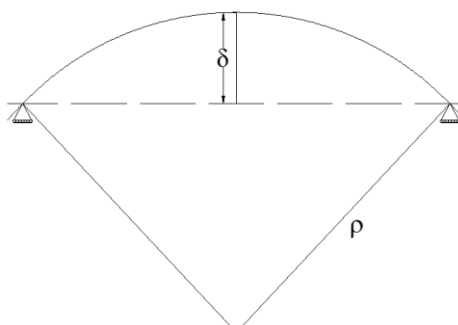


Figure 5.15 – Connection between the Bend radius and the half span displacement

The comparison of the displacements between the analytical and the numerical approach may be found below:

	Analytical	Numerical
$\delta_{\text{midspan,PS}}$	0.735 mm	0.712 mm
Δ		3%

As the difference is nearly 3% the variation of temperature equivalency can be assumed.

5.10 Loading Step

To avoid to perform an explicit analysis in two steps, i.e., pre-stress step and loading step, it was chosen to run this step on a different analysis and then run the second step in another job with an imported predefined field containing the stress on each element from the 1st step. To do so, according to (Abaqus, 2012), it was necessary to change the element family, i.e., the element instead of being part of the usual shell family became part of the coupled temperature-displacement family. Thus, the stress field due to the pre-stress tension was then transferred to the loading step as a predefined stress field.

5.11 Materials' Properties

5.11.1 Adhesive Properties

The adhesive used in the experimental tests (Araldyte 2047-1) has a non-linear law with ν of 0.43. (Nhamoinesu and Overend, 2012), established an analytical expression to characterize the behaviour of the referred adhesive.

$$\begin{cases} \sigma = -16881 \cdot \varepsilon^2 + 766.43 \cdot \varepsilon + 0.1548 & \varepsilon \leq 0.025 \\ \sigma = -1300.5 \cdot \varepsilon^2 + 141.34 \cdot \varepsilon + 6.3631 & \varepsilon > 0.025 \end{cases} \quad (5.14)$$

Where σ and ε stand for stress [MPa] and extension, respectively. For the numerical model a multi-linear curve was used to reproduce the adhesive non-linear law. In order to save resources, two different curves were tested. Figure 5.16a) shows the referred curves. Figure 5.16b) shows a comparison of the numerical results for both curves.

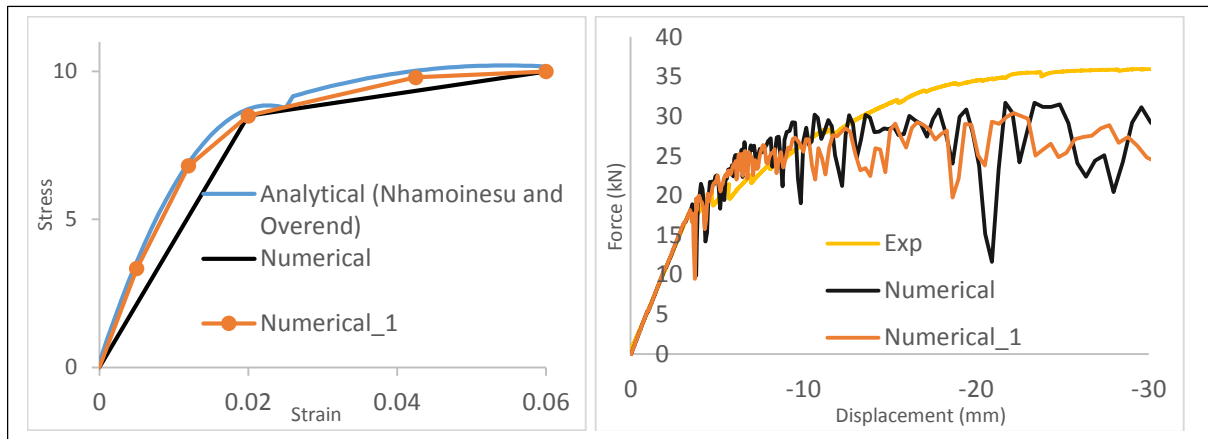


Figure 5.16 - Adhesive Behaviour Study

According to the numerical calculations these two different approaches resulted in similar load-displacement plots, as it can be observed by Figure 5.16. For this reason, and to make the calculations less complex, only the first simpler approach was considered in the following numerical models.

5.11.2 Steel Properties

The Steel used, as it has been told, is a stainless steel. Stainless Steel AISI 304 (1.4301) in particular. Its properties may be found in 4.3.2.

Uniaxial coupon tests on the steel have not yet been performed for the batch of AISI304 used for the steel strips used in the experimental campaign. Nevertheless, the results of uniaxial tests on an actual batch of AISI304 were used for the numerical analysis.

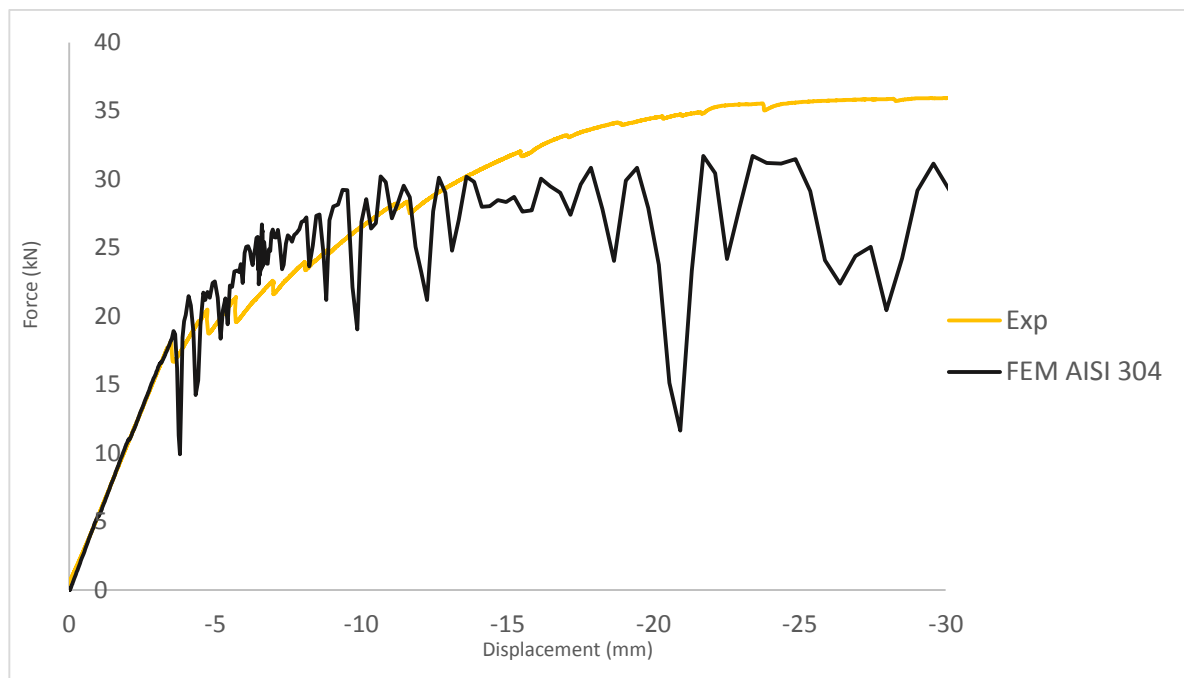


Figure 5.17 – Comparison between the experimental results and the FEM results with the Steel characterization according to Louter, 2011

Comparing the results (Figure 5.17) it is visible the similarities between the experimental results and the numerical results. Thus, the steel behaviour in the upcoming models was done according to the uniaxial tests performed in Louter, 2011.

5.11.3 Glass Properties

The elasticity of the glass in the numerical modelling was defined with a Young's Modulus of 70 GPa and a Poisson's ratio of 0.23 (Louter, 2011). The post-cracking behaviour was defined by entering the failure stress and the Mode I fracture energy. The failure stress was established from the experimental results. (see 4.3.1)

5.11.3.1 Mode I fracture Energy

The crack initiation is defined by the critical displacement in order to reach the cracking. That critical displacement is dependent on the Mode I fracture energy (Figure 5.18).

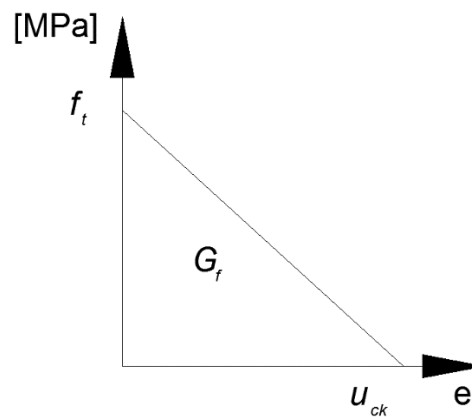


Figure 5.18 - Mode I fracture Energy (Area)

From Figure 5.18, the critical displacement, u_{ck} , is given by:

$$G_f = f_t \times u_{ck} \times \frac{1}{2} \Leftrightarrow u_{ck} = \frac{2G_f}{f_t} \quad (5.15)$$

In linear elastic Fracture Mechanics there are three fracture modes (Lawn, 1993). All of them may be defined as:

- Mode I – normal separation of the crack walls under the action of tensile stress
- Mode II – longitudinal shearing of the crack walls in a direction normal to the crack front
- Mode III – lateral shearing parallel to the crack front

These different fracture modes may be also summarized into this figure that follows:

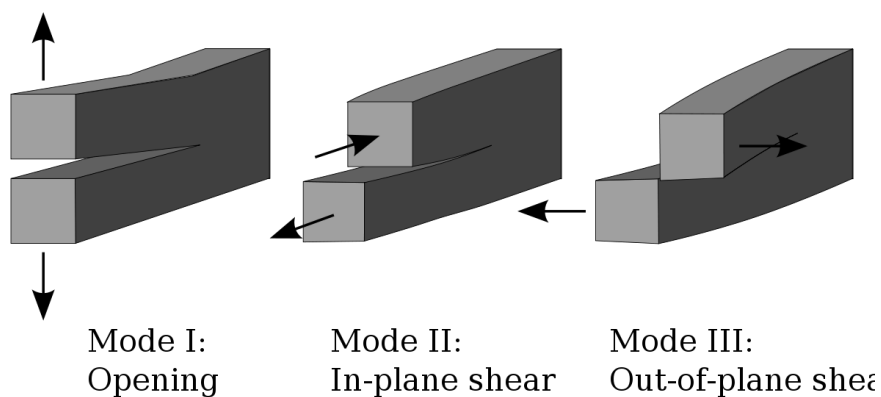


Figure 5.19 - Different Fracture Modes (Twisp, 2008)

For the structural model being studied, only mode I is relevant (see Figure 5.20) since there are only forces at the plane of the structure (longitudinal).

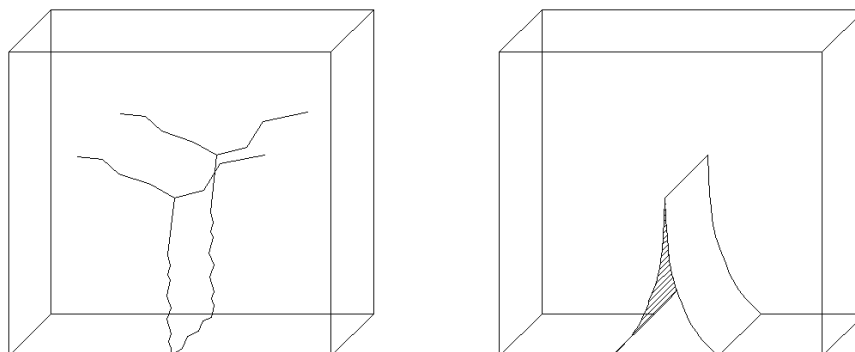


Figure 5.20 – Mode I fracture energy in glass

The Mode I fracture Energy in the bibliography varies between 3 J/m^2 (Louter, 2011) and 8 J/m^2 (Bernard et al., 2013). A study in (Bedon and Louter, 2014) was done regarding this parameter and the conclusion is that, despite the global resistance and structural performance of the examined beams not being affected by the variation in Mode I Fracture Energy of glass, the fracture pattern indeed varies significantly. In this study it was concluded that the lower the fracture energy the more cracks appeared in glass and vice-versa. In Figure 5.21 it can be observed what was said before.

Table 5.3 – Fracture Energy study done in (Bedon and Louter, 2014)

<u>FEM</u>	<u>Mode I fracture Energy</u>
M01	3 J/m^2
M-GF02	8 J/m^2
M-GF03	5.5 J/m^2

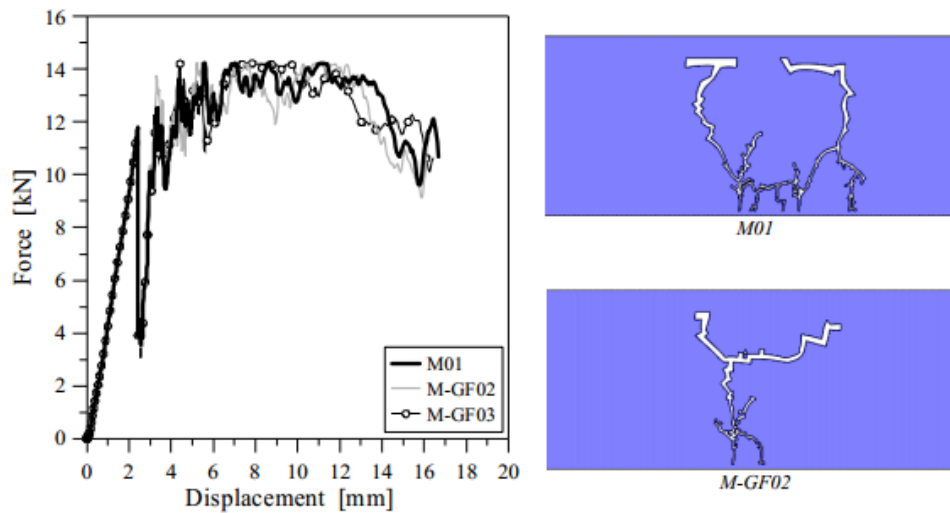


Figure 5.21 – Effects of fracture energy of glass. Comparison of load-displacement plots [left]; Comparison of crack patterns [Right] (Bedon and Louter, 2014)

As in this theses the main goal is to achieve a plausible and credible structural behaviour of the glass beam and not so much an exact and precise fracture pattern, the mode I fracture energy was assumed as 3 J/m^2 .

In order to characterize the damage evolution several other parameters are needed, namely the one defining brittle shear and brittle failure. (Abaqus, 2012) Both parameters are looked into in the next section.

5.11.3.2 Brittle Shear

The shear behaviour is based on the common observation that the shear behaviour depends on the amount of crack opening. More specifically, the cracked shear modulus is reduced as the crack opens. Therefore, Abaqus offers a shear retention model in which the post-cracked shear stiffness is defined as a function of the opening strain across the crack. (Abaqus, 2012)

$$G_c = \rho \cdot G \quad (5.16)$$

Where G_c , ρ and G stand for post-cracking shear modulus, shear retention factor and shear modulus, respectively.

The brittle shear retention, ρ , varies between 0 and 1; whereas 0 meaning no shear retention thus full reduction in shear modulus and 1 meaning no reduction at all. This parameter was already studied in Louter, 2011 and in the conclusions of this study it could be read that when this parameter was too high (1) it showed highly extensive cracking and when it was too low (nearly 0) it shown a limited number of cracks. For the particular experiment the most suitable value was 0.01. Nevertheless, and since the numerical modelling in Louter, 2011 was done in the software DIANA, and so it wasn't done in the same software used for the numerical modelling of this dissertation, it was done a study of this parameter.

It should also be noticed that this value is dependent on the crack strain so it was needed to define a function where the shear retention varies with the crack strain as in the example seen in Figure 5.22. (Abaqus, 2012).

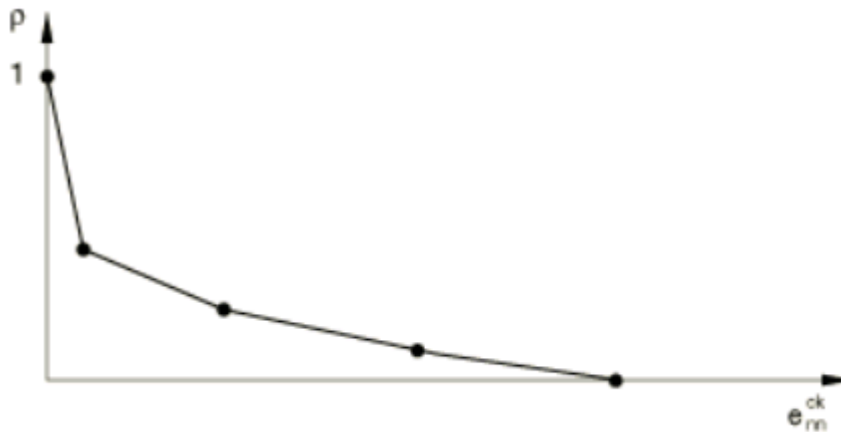


Figure 5.22 - Shear Retention Factor (ρ) varies with Crack Strain Opening (e^{ck})

Abaqus offers two methods to define the brittle shear. One method is by using a piecewise linear form (just like in Figure 5.22) and the other is in power law form in which the shear retention factor varies in uni-linear form (Equation 4.9). Although the parameters to input are different, both methods characterize the shear behaviour in the same way. Any power law form can be characterized in a piecewise linear form. To define the brittle shear a power law form was selected:

$$\rho(e_{nn}^{ck}) = \left(1 - \frac{e_{nn}^{ck}}{e_{max}^{ck}}\right)^p \quad (5.17)$$

Where ρ , e_{nn}^{ck} , e_{max}^{ck} and p stand for shear retention factor, crack strain, maximum crack strain and power, respectively.

In order to establish the sensitivity of the FEA to this parameter and to select its most adequate value for the calibration at hand, a comparative analysis was performed. (Table 5.4 and Figure 5.23)

Analysis	p	e_{\max}^{ck}
FEM p=1 $e_{\max}^{\text{ck}}=0.1$	1	0.1
FEM p=1 $e_{\max}^{\text{ck}}=0.01$	1	0.01
FEM p=2 $e_{\max}^{\text{ck}}=0.1$	2	0.1
FEM p=1 $e_{\max}^{\text{ck}}=0.01$	2	0.01
FEM p=3 $e_{\max}^{\text{ck}}=0.1$	3	0.1

Table 5.4 – Shear Retention Factor parameter variation

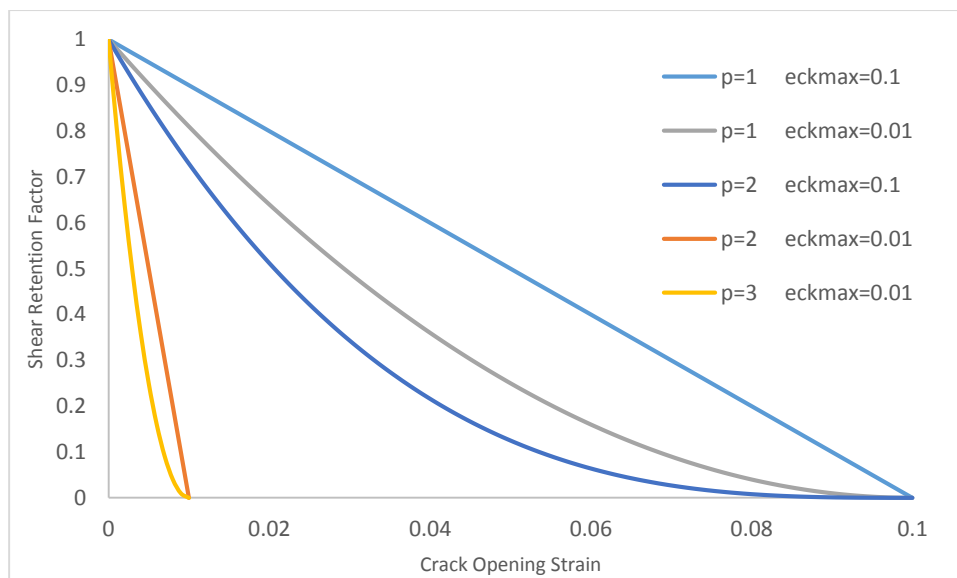


Figure 5.23 – Shear retention factor parameter study

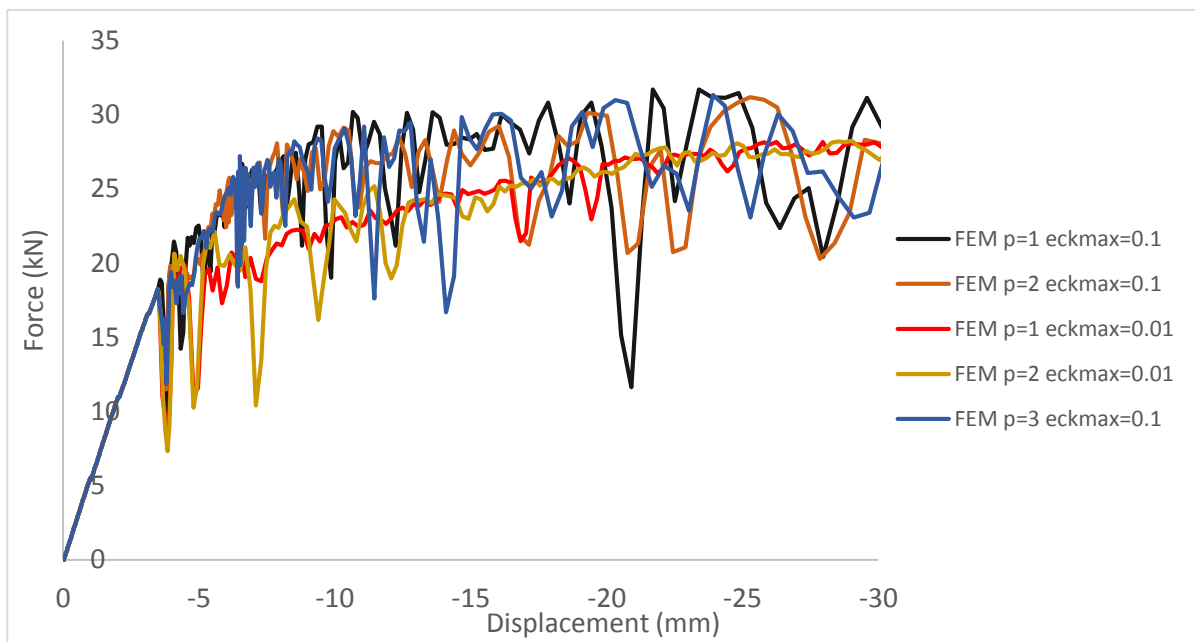
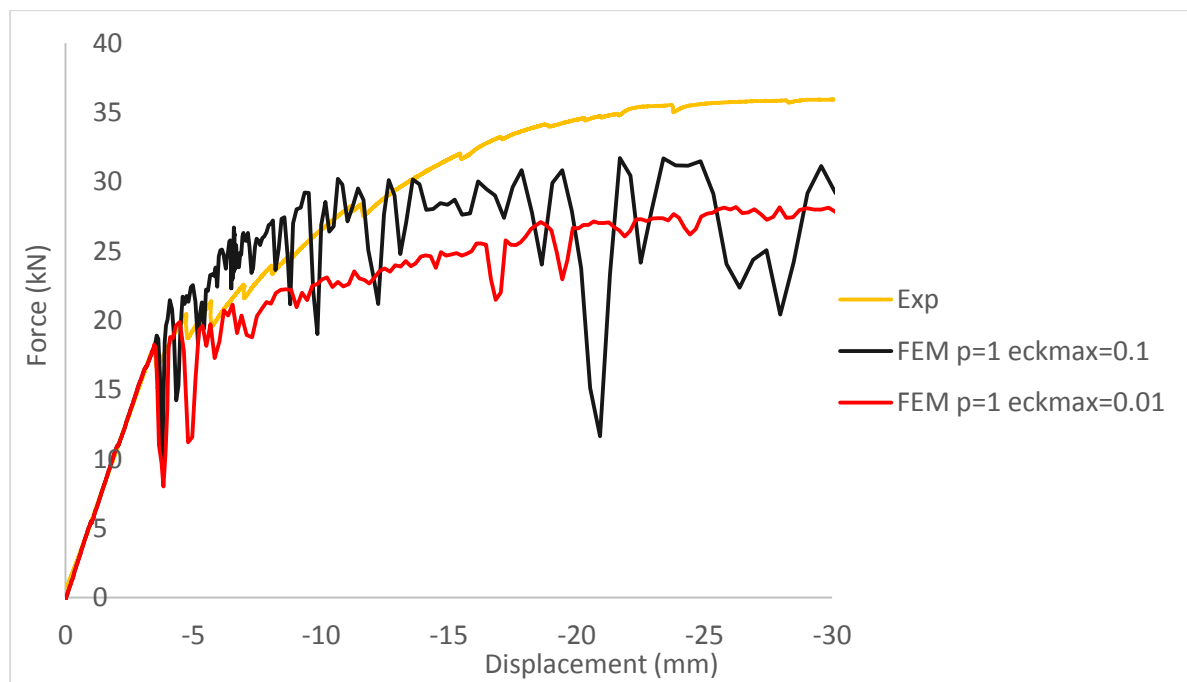


Figure 5.24 - Shear Retention Factor study

After running these analysis, and analysing the Figure 5.24 it was concluded that the power, p , doesn't have much influence in the analysis. Regarding the maximum crack strain, e_{max}^{ck} , the differences are visible; being the analysis a little stiffer than that of the experiment when $e_{max}^{ck} = 0.1mm$, and being less stiff when $e_{max}^{ck} = 0.01mm$ as it is visible in Figure 5.25. For that reason it was also done an analysis in which $e_{max}^{ck} = 0.05mm$.

Figure 5.25 - Influence of the e_{max}^{ck}

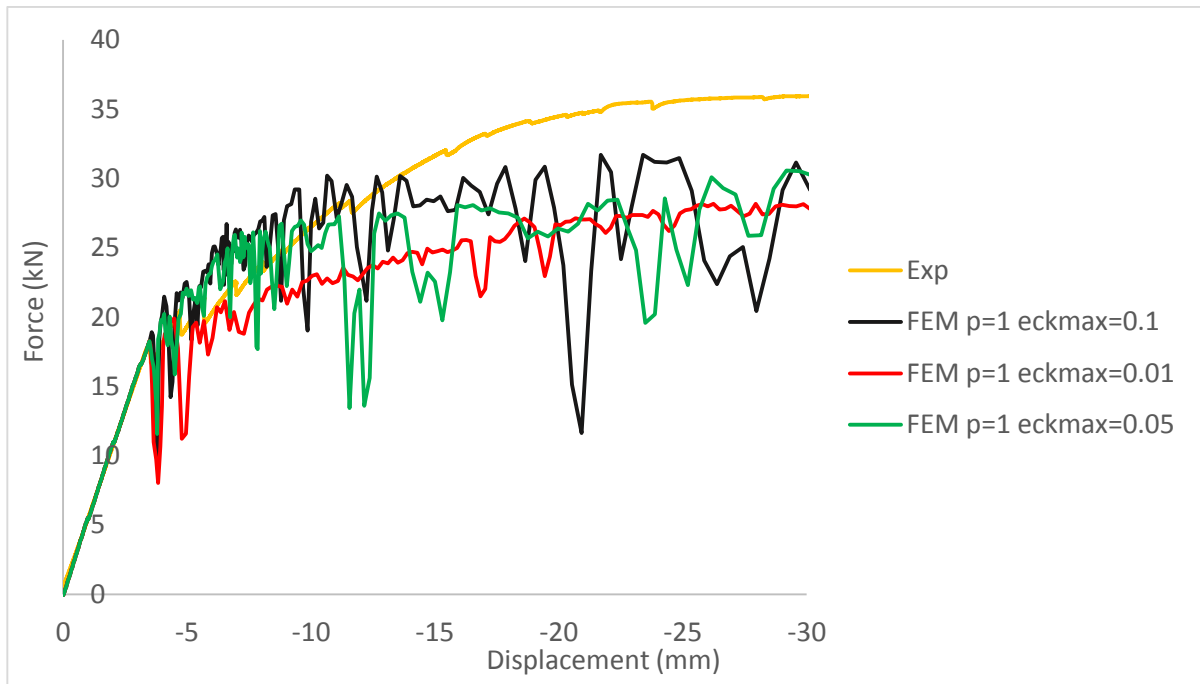


Figure 5.26 - Comparison between $e_{max}^{ck}=0.1$, $e_{max}^{ck}=0.01$ and $e_{max}^{ck}=0.05$

The analysis in which $e_{max}^{ck} = 0.05mm$ was slightly different from that of the $e_{max}^{ck} = 0.1mm$ as it can be observed in Figure 5.26, meaning that this parameter should be smaller. An analysis with $e_{max}^{ck} = 0.04mm$ was done. As this analysis was too similar to the one with $e_{max}^{ck} = 0.04mm$ as it can be observed in, from now on all the models should be done with $e_{max}^{ck} = 0.04mm$ because it's less complex and therefore the computational cost is lower.

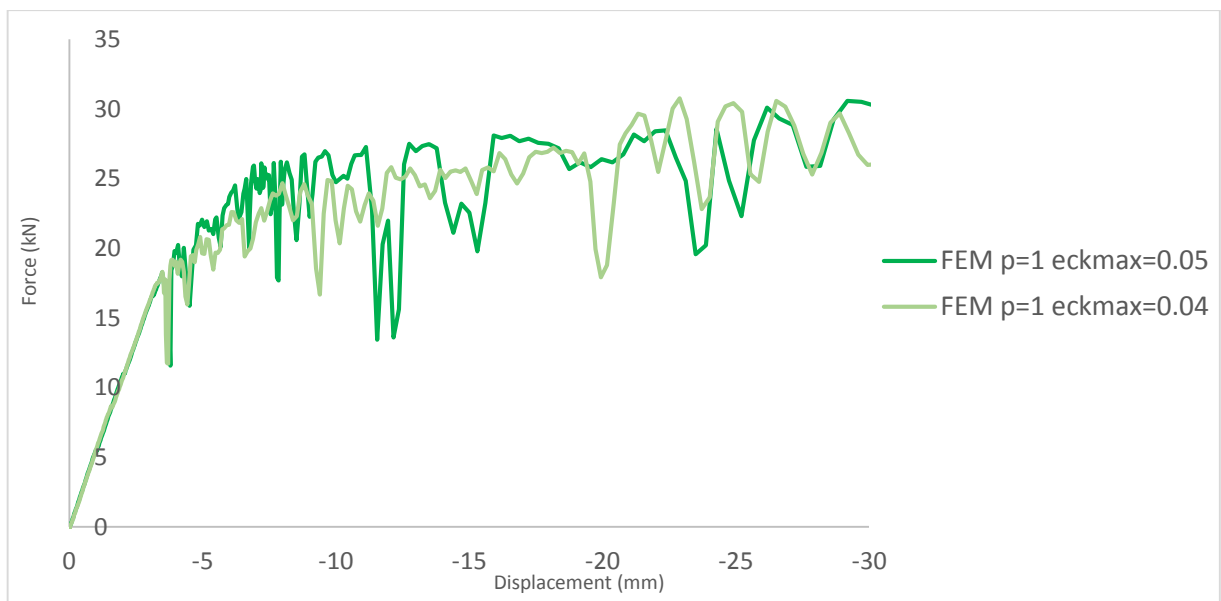


Figure 5.27 - Difference between $e_{max}^{ck}=0.05$ and $e_{max}^{ck}=0.04$

5.11.3.3 Brittle Failure

When the direct cracking displacement reaches the value defined as the failure displacement, the element node fails and all the stress components are set to zero. If all of the material points in an element fail, the element is removed from the mesh. (Abaqus, 2012)

To model the failure of the model in a rudimentary way, Abaqus has a capability called “Brittle Failure” criterion. This feature helps in computations by removing an element that can no longer carry stress. By removing these elements it can be assured that there isn’t the excessive distortion of those elements and subsequent premature termination of the simulation. This feature should be handled with care given the fact that whenever the brittle material loses its ability to carry tensile forces does not preclude it from withstanding compressive stresses. Therefore, if a material is expected to carry loads after it has failed in tension it’s not appropriate to remove those elements. (Abaqus, 2012)

The following sentence may be found in Abaqus manual (Abaqus, 2012): “Thus, the effective use of the brittle failure criterion relies on you having some knowledge of the structural behavior and potential failure mechanism. The use of the brittle failure criterion based on an incorrect user assumption of the failure mechanism will generally result in an incorrect simulation.”

In order to simplify the numerical modelling the brittle failure was set to be at the moment when the shear retention factor got to zero, i.e., the Brittle Failure was equal to e_{max}^{ck} in all analysis. This also goes according to the suggestion given in Abaqus, 2012 regarding the shear retention factor in which it says that “Zero shear retention should not be used”.

6 Parametric Study

In order to increase the load-bearing capacity of the post-tensioned glass beam, key parameters were studied in this document. More parameters could have been studied such as the pre-stress force used – since the yield strength of the steel is much higher than 200 MPa which is the value given in (Ruukii, 2014) - different types of adhesives or simply different dimensions for the beam. Such studies are not present in this thesis due to the time and resources limitations.

This chapter regards the study of two different thicknesses of the adhesive and two different characterizations of the steel. To perform this study the models were calculated with the definitions found in Chapter 5.

6.1 Thickness of the Adhesive

Two thicknesses were chosen; one which the thickness is increased by 25% and another which the thickness is decreased by 25%. (Table 6.1). The results of the numerical modelling regarding the calculations with the different thicknesses of the adhesive are shown in Figure 6.1.

Table 6.1 – Thicknesses of the Adhesive studied

t_{adhesive}	
100% (Original)	1.5 mm
125%	1.875 mm
75%	1.125 mm

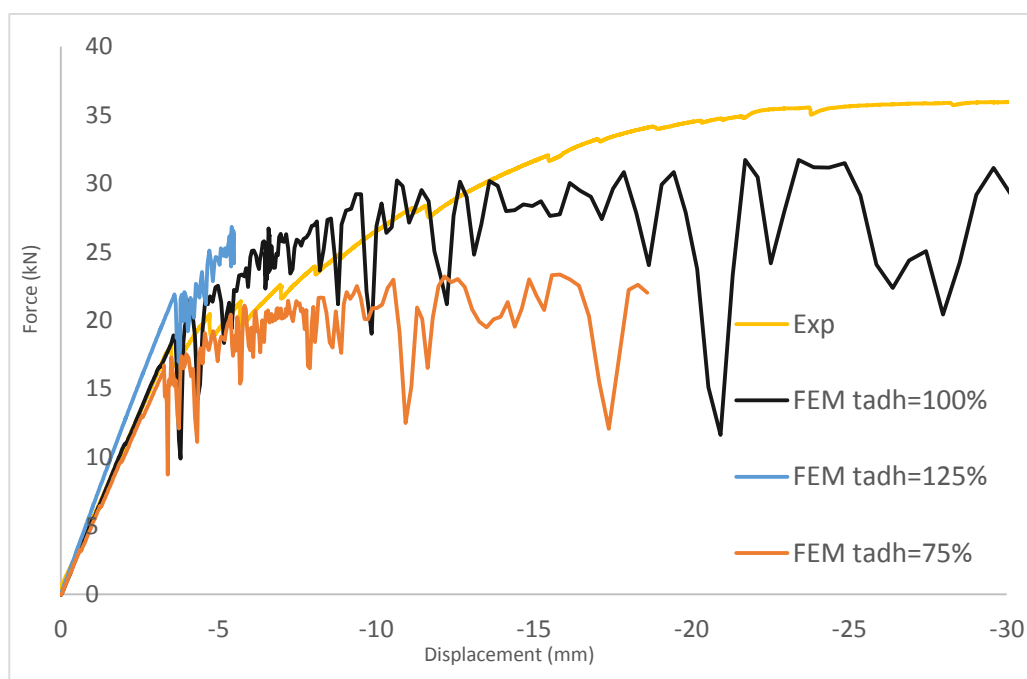


Figure 6.1 – Results of the parameter study regarding the thickness of the adhesive

By analysing Figure 6.1 it is notorious the influence of the thickness of the adhesive. When the adhesive increases the whole bending stiffness of the system increases. This is due to the increase of the distance between the steel and the centre of mass of the beam.

Table 6.2 – First Crack and maximum load of the thickness of the adhesive study

Analysis	First Crack	Δ_{FC}	Max Load	Δ_{ML}
Exp	18.4 kN	-	37 kN	-
FEM $t_{adh}=100\%$	18.2 kN	-	31.71 kN	-
FEM $t_{adh}=125\%$	21.5 kN	18%	-	-
FEM $t_{adh}=75\%$	16.0 kN	-12%	23.34 kN	-26%

6.2 Characterization of the Steel

In order to assess the influence of the yield stress of the steel, two types of steel were chosen. One in which the yield stress is increased by 25% and another in which the yield stress is decreased by 25%. The results of the numerical modelling regarding the calculations with the different characterizations of the steel are shown in Figure 6.2.

Table 6.3 – Steel study

$\sigma_{y,steel}$	
100% (Original)	550 MPa
125%	687.5 MPa
75%	412.5 MPa

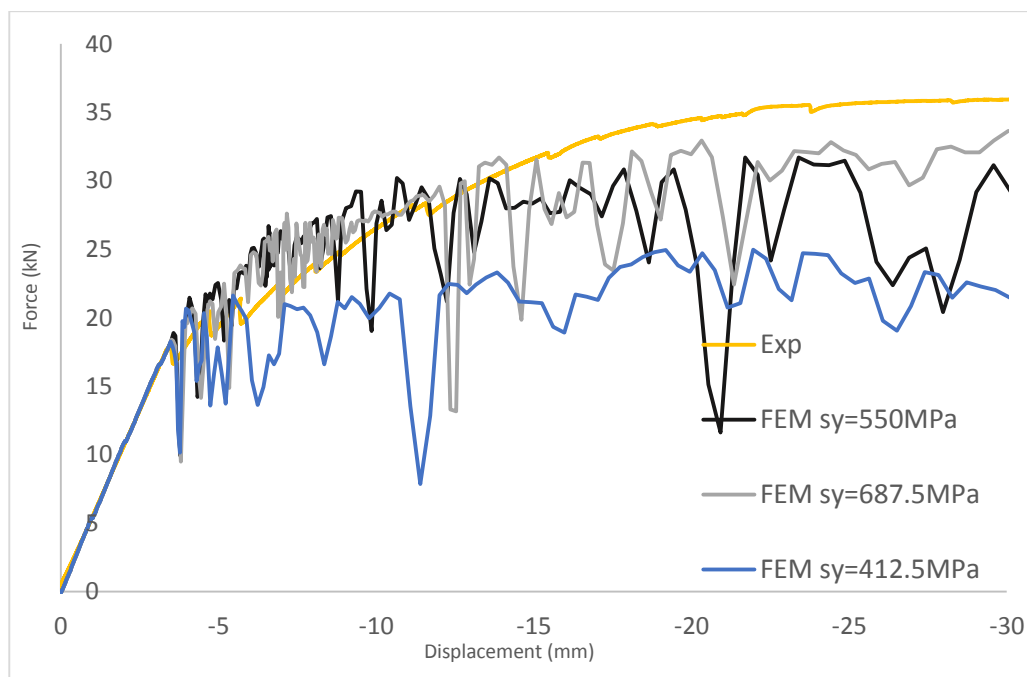


Figure 6.2 - Results of the parameter study regarding the characterization of the steel

Table 6.4 - Initial failure and maximum load of the steel characterization study

Analysis	Initial Failure	Δ	Max Load	Δ
Exp	18.4 kN	-	37 kN	-
FEM $\sigma_y=550$ Mpa	18.2 kN	-	31.71 kN	-
FEM $\sigma_y=687.5$ Mpa	18.2 kN	0%	34.0182	7%
FEM $\sigma_y=412.5$ Mpa	18.2 kN	0%	24.98 kN	-21%

By analysing Figure 6.2 it can be concluded that a steel with a yield stress of 412.5 MPa is unadvised because it lowers significantly the resistance of the beam. However the increase of the yield stress to 687.5 MPa almost doesn't change the response of the beam, i.e., the improvement is less than 10%. Thus, the use of the AISI 304 is highly advised.

7 Conclusions

The purpose of this thesis is the characterization of a specific type of post-tensioned glass beams. This thesis aimed to contribute to the whole knowledge of a relatively new, feasible and advantageous product.

The main focus of the thesis was on the preparation of the Finite Element Modelling. The Finite Element Analysis, as it was proven, represents the experimental results which means that the correlation between numerical data and experimental data may be obtained. In that Finite Element Analysis it's shown that the software used is highly sensitive to some input parameters and that a significant number of increments are needed. Thus, the machine to perform these calculations should have high performance settings.

From the parametric study it can be concluded that the increase of thickness of the adhesive is beneficial so the beam can bear more load, for instance, when the thickness of the adhesive increases 25%, the first crack only occurs to 21.5 kN which is a load 18% higher than that of the previous analysis. Regarding the steel characterization it was shown that for a steel in which the yield stress was higher 25% the maximum load the beam could bore was only 7% higher than that of the experiments. Thus, the steel used in the experimental campaign may have the optimal characteristics.

Regarding the pre-stress within the numerical modelling, given that the used software didn't have a built-in function regarding this matter, in order to get an accurate stress distribution on the steel, a variation of temperature of $\frac{N}{EA} \times \frac{1}{\alpha}$ should be used, being N the wanted value of pre-stress. The variation of temperature has proven to be the most suitable when compared to the usual force analogy.

7.1 Suggestions for future research

The study on post-tensioned glass beams is not over. To overcome the difficulties of these beams, more parameters should be studied as it was written before. After the completion of that study a software can be made in which the user input the load the beam should load and from an algorithm it should give the user a range of possibilities regarding these parameters that could fulfil the user's needs. Last but not least, this study can and should be implemented in the next European Norm exclusively about glass.

8 Bibliographic References

- Abaqus Online Documentation (2012), generated on Monday, February 13, 2012 at 14:58:02.
Dassault Systèmes
- Abaqus 6.13 (2013), “Getting Started with Abaqus: Interactive Edition”
- Bedon, C, Louter, C. (2014). “Parametric 2D numerical investigation of the structural response of SG-laminated reinforced glass beams”. Challenging Glass 4 & Cost Action TU0905 Final Conference, pp. 483-490.
- Belis, J., Van Hulle, A., Out, B., Bos, F., Callewart, D., Poulis, H. (2011). “Broad screening of adhesives for glass-metal bonds”. Proceedings of Glass Performance Days, pp. 286-289.
- Bernard, F., Krour, B., Benyoucef, S., Fahsi, B. (2013). “Analysis of the debonding risks and the failure of laminated glass thanks to a coupled analytical-numerical investigation”. COST Action TU0905 & Mid-term Conference on Structural Glass, pp. 391-403.
- Carter, C., Norton, M. (2007). “Ceramic Materials, Science and Engineering”. 1st Edition. London, United Kingdom
- Copeland, P., Martin, J. (1981). “Story of Glass”. 1st Edition. New York, United States of America
- Dias da Silva, V. (2004). “Mecânica e Resistência dos Materiais”. 3rd Edition. Coimbra, Portugal
- Diaz, M., Miguel, J., Aguirregabiria, B. (2011). “Prestresses Glass Beams”. Glass Performance Days 2011, pp. 645-649
- Feldmann, M., Kasper, R. (2014). “Guidance for European Structural Design of Glass Components”. Luxembourg, Luxembourg
- Froli, M., Lani, L. (2010). “Glass tensegrity trusses”. Structural Engineering International 2010, pp. 436-441
-

-
- Froli, M, Mamone, V. (2014). “A 12 meter long segmented post-tensioned steel-glass beam (TVT gamma). Challenging Glass 4 & Cost Action TU0905 Final Conference, pp. 243-251.
- Haldimann, M., Luible, A., Overend, M. (2008), “Structural Use of Glass”. Zurich, Switzerland
- Huntsman (2013). Araldite 2047-1, Methacrylate adhesive requiring minimal surface pretreatment. Technical data sheet.
- Jordão, S., Pinho, M., Martins, J.P, Santiago, A. (2014), “Numerical modelling of laminated glass beam reinforced with pre stressed cables”. Challenging Glass 4 & Cost Action TU0905 Final Conference, pp. 253-260.
- Kennedy, R. (1997), “The History and the Future of the Flat Glass Industry”. Glass Processing Days, pp. 28-36.
- Lawn, B. (1993). “Fracture of Brittle Solids”. 2nd Edition. Cambridge, United Kingdom.
- Louter, C. (2011). “Fragile yet Ductile, Structural Aspects of Reinforced Glass Beams”. PhD Thesis. Technische Universiteit Delft
- Louter, C. (2013). “Reinforced and post-tensioned glass beams”. Glass Performance Days 2013, pp. 353-355.
- Louter, C., Nielsen, J.H. (2013). “Numerical analysis of the effect of SG-interlayer shear stiffness on the structural performance of reinforced glass beams. COST Action TU0905 & Mid-term Conference on Structural Glass, pp. 405-412
- Mashayekhi@ 2013.
<http://mashayekhi.iut.ac.ir/sites/mashayekhi.iut.ac.ir/files//u32/presentation4.pdf>.
Slides from a FEM classroom taken from the website of Professor Dr. Mohammad Mashayekhi
- Nhamoinesu, S., Overend, M. (2012). “The Mechanical Performance of Adhesives for a Steel-Glass Composite Façade System” Challenging Glass 3 – Conference on Architectural Structural Applications of Glass, pp. 293-306
-

-
- Reynolds, L. @ (2009), <https://www.flickr.com/photos/lwr/3558879983/>. Crown Glass photo found in flickr (Website consulted on Nov 15, 2013)
- Ruukki@ (2014). <http://www.ruukki.com/Products-and-solutions/Stainless-steel-and-aluminium-products/Stainless-steel-flat-products/Stainless-steel-1430114307-cold-rolled>. Stainless steel 1.4301/1.4307 cold-roller Properties (Website consulted on Feb 25, 2014)
- Stelzer, I. (2010). “High Performance Laminated Glass”. Challenging Glass 2 – Conference on Architectural and Structural Applications of Glass, pp. 467-474
- Twisp’s Wikipedia@ (2008). http://commons.wikimedia.org/wiki/File:Fracture_modes_v2.svg. Three fracture modes. (Website consulted on Jun 27, 2014)
- Valarinho, L. (2010). “Construção em Vidro Estrutural, Comportamento estrutural de vigas mistas vidro-GFRP”. Tese de Mestrado. Instituto Superior Técnico, Lisboa.
- Weller, B., Engelmann, M. (2014). “Deformation of Spannglass beams during post-tensioning”. Challenging Glass 4 & Cost Action TU0905 Final Conference, pp. 285-294.
- Wurm, J. (2007). “Glass Structures: Design and Construction of Self Supporting Skins”. Basel, Boston, Berlin